Driftsonde observations to evaluate numerical weather prediction of the late 2006 African monsoon

Philippe Drobinski, Fatima Karbou, P. Bauer, P. Cocquerez, C. Lavaysse, T. Hock, D. Parsons, Florence Rabier, Jean-Luc Redelsperger, S. Vénel

Driftsonde Observations to Evaluate Numerical Weather Prediction of the Late 2006 African Monsoon

PHILIPPE DROBINSKI,* FATIMA KARBOU,+ PETER BAUER,# PHILIPPE COCQUEREZ,@ CHRISTOPHE LAVAYSSE,& TERRY HOCK,** DAVID PARSONS,**,++ FLORENCE RABIER,## JEAN-LUC REDELSPERGER,## AND STÉPHANIE VÉNEL@

* *Laboratoire de Météorologie Dynamique, Institut Pierre Simon Laplace, École Polytechnique/CNRS, Palaiseau, France*
+ *CNRM-GAME, Météo-France/CNRS, St Martin d'Hères, France*
# *European Centre for Medium-Range Weather Forecasts, Reading, United Kingdom*
@ *Centre National d'Études Spatiales, Toulouse, France*
& *Department of Atmospheric and Oceanic Sciences, McGill University, Montreal, Quebec, Canada*
** *National Center for Atmospheric Research, Boulder, Colorado*
CNRM-GAME, Météo-France/CNRS, Toulouse, France

(Manuscript received 22 July 2011, in final form 8 October 2012)

ABSTRACT

During the international African Monsoon Multidisciplinary Analysis (AMMA) project, stratospheric balloons carrying gondolas called driftsondes capable of dropping meteorological sondes were deployed over West Africa and the tropical Atlantic Ocean. The goals of the deployment were to test the technology and to study the African easterly waves, which are often the forerunners of hurricanes. Between 29 August and 22 September 2006, 124 sondes were dropped over the seven easterly waves that moved across Africa into the Atlantic between about 10° and 20°N, where almost no in situ vertical information exists. Conditions included waves that developed into Tropical Storm Florence and Hurricanes Gordon and Helene. In this study, a selection of numerical weather prediction model outputs has been compared with the dropsondes to assess the effect of some developments in data assimilation on the quality of analyses and forecasts. By comparing two different versions of the Action de Recherche Petite Echelle Grande Echelle (ARPEGE) model of Météo-France with the dropsondes, first the benefits of the last data assimilation updates are quantified. Then comparisons are carried out using the ARPEGE model and the Integrated Forecast System (IFS) model of the European Centre for Medium-Range Weather Forecasts. It is shown that the two models represent very well the vertical structure of temperature and humidity over both land and sea, and particularly within the Saharan air layer, which displays humidity below 5%–10%. Conversely, the models are less able to represent the vertical structure of the meridional wind. This problem seems to be common to ARPEGE and IFS, and its understanding still requires further investigations.

1. Introduction

Over the annual cycle, precipitation events in the tropical regions of West Africa are extremely intense during summer. Rainfall events during the dry season, although rare, can have a significant impact locally (Knippertz and Fink 2008, 2009). The annual rainfall cycle over West Africa is linked to the variability of the West African monsoon (WAM) system associated with major changes in the atmospheric circulation over the region (Sultan and Janicot 2003). The region is characterized by an African easterly jet (AEJ), which develops at about the 600-hPa pressure level at a location of 4°–5°N latitude in winter, strengthens and migrates to 15°N, its highest position, in August, and quickly transits back toward the equator in the autumn (Nicholson and Grist 2003). This jet develops because of heating of the West African landmass during summer that creates a low-level temperature gradient from the Gulf of Guinea and the Sahara with the atmospheric response is to generate vertical wind shear to maintain thermal wind balance. African easterly waves (AEW)—which are

++ Current affiliation: School of Meteorology, University of Oklahoma, Norman, Oklahoma.

Corresponding author address: Philippe Drobinski, Laboratoire de Météorologie Dynamique, École Polytechnique, Route de Saclay, 91128 Palaiseau CEDEX, France.
E-mail: philippe.drobinski@lmd.polytechnique.fr

DOI: 10.1175/JAMC-D-11-0176.1

synoptic-scale, westward-propagating disturbances produced by barotropic and baroclinic instabilities embedded in the AEJ—modulate the convective activity over the region (Payne and McGarry 1977; Fink and Reiner 2003; Mekonnen et al. 2006). It should be noted that recent publications highlight the relatively important role of finite-amplitude initial perturbations in the initiation and development of AEWs (see, e.g., Berry and Thorncroft 2005; Hall et al. 2006; Leroux et al. 2010; Thorncroft et al. 2008). A small number of mesoscale storm systems associated with the AEJ develop into tropical cyclones after they move from West Africa into the tropical Atlantic Ocean, mainly during August and September (Cook 1999). The annual WAM cycle is first characterized by the onset stage, which is linked to an abrupt latitudinal shift of the intertropical convergence zone (ITCZ) from a quasi-stationary location at 5°N in May–June to a second quasi-stationary location at 10°N in July–August (Sultan and Janicot 2003; Drobinski et al. 2005, 2009; Ramel et al. 2006; Sijikumar et al. 2006; Hagos and Cook 2007; Sultan et al. 2007; Janicot et al. 2008). The second transition phase corresponds to the WAM withdrawal period from mid-August to mid-October and is comparatively less investigated than the WAM onset and mature stages. The late WAM period corresponds to a decrease of convective activity, a warming of the tropical Atlantic Ocean, and the beginning of the hurricane period during which tropical cyclones often develop from convective perturbations embedded within AEWs (Carlson 1969).

The West African societies are highly vulnerable to the monsoon rainfall variability. Therefore, accurate and reliable prediction of the WAM stages as well as a good forecast of the associated meteorological events (convection, dust storms) is a key scientific challenge and societal issue. Not surprisingly, a realistic representation of the African monsoon in the models is a major scientific challenge because it involves a proper consideration of all the mechanisms that govern the monsoon. For example, despite the tremendous progress made in recent years, the NWP models are still unable to fully reproduce the hydrological cycle, especially in the tropics (Meynadier et al. 2010b). The NWP weaknesses reflect gaps in model physics exacerbated by the lack of observations assimilated in these areas. Data quality is also an issue, particularly that of the very few radiosonde observations assimilated in tropical regions. Studies have shown that they accentuate the well-known rainfall bias in the tropics because of their own humidity bias (Nuret et al. 2008). The radiosondes are still the baseline data for numerical weather prediction models and potential biases affecting these observations can be propagated to the outputs of the NWP models including the rain forecasts. Not surprisingly, it is still challenging to appropriately predict the monsoon onset, duration, and intensity as most models have an incomplete representation of the monsoon system, mainly because of lack of adequate parameterizations that can translate the complex physical processes involving the water cycle in West Africa (Tompkins and Feudale 2010). Moreover, Nuret et al. (2008) showed that a dry radiosonde bias in the Sahel region may have a significant impact on the diurnal cycle of total column water vapor (TCWV) and of convective available potential energy (CAPE) and therefore on the life cycle of convective systems. This would result in a southward shift of the ITCZ in the European Centre for Medium-Range Weather Forecasts (ECMWF) model with a dry rainfall bias over the Sahel. Faccani et al. (2009) showed that correcting the humidity bias of radiosonde following the method developed by Agusti-Panareda et al. (2009) led to better rainfall forecasts over Africa. Impact studies targeting the assimilation of more observations in the tropics, coming from in situ (Faccani et al. 2009; Agusti-Panareda et al. 2010) or remote sensing instruments (Bauer 2009; Karbou et al. 2010), put forward an improvement in analyses/forecasts due to the use of these additional observations. Indeed, the conclusions of Andersson et al. (2007) predicted at that time the beneficial contribution of observations of moisture for better atmospheric analyses and forecasts. One result of this study was the ability of current assimilation systems to extract useful information from observations of moisture. This can be achieved thanks to advances in data assimilation techniques, to a better use of satellite observations, and to improved physical parameterizations.

If more work is carried out to increase the realism of models, the evaluation of the models remains difficult, especially in such key regions. Assessment protocols exist in several NWP centers but rarely make use of data independent of the assimilation. Given the availability of observations during some measurement campaigns, we draw attention to opportunities for partial evaluation of models. Apart from other potential scientific results, such work would highlight the value of measurements during field campaigns for which preparation can take several years and funding is often difficult to obtain.

Given the societal importance and challenge of predicting the WAM, the African Monsoon Multidisciplinary Analysis (AMMA) program was initiated in 2002, including an intensive field phase in 2006 (Redelsperger et al. 2006). During AMMA, drifting balloons were launched from Zinder (Niger) (Fig. 1) into the stratosphere (about 50 hPa) and dropped 124 dropsondes over wide swaths of Africa and the Atlantic Ocean, where almost no in situ vertical information exists, between

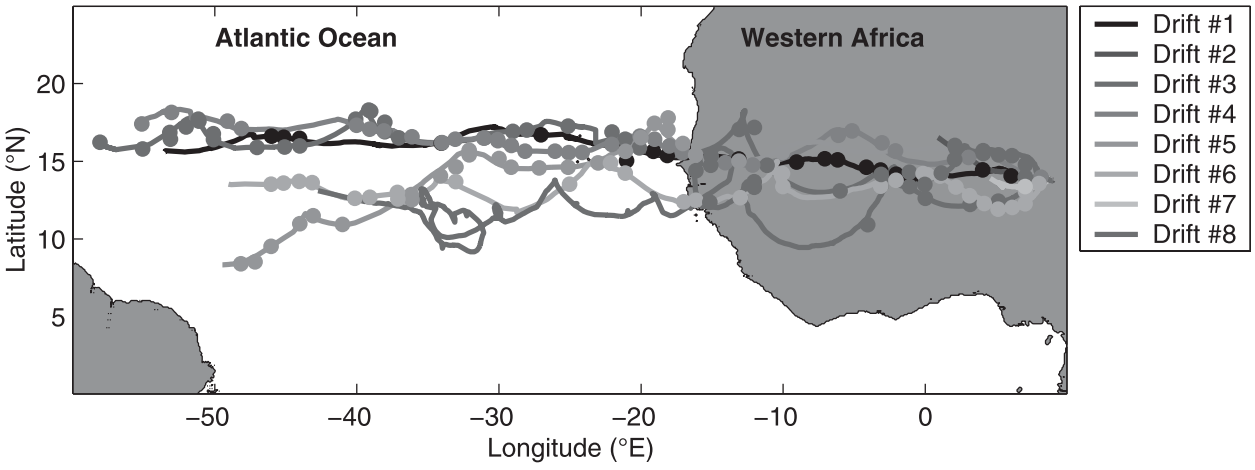

FIG. 1. Trajectories of the eight driftsondes launched from Zinder (Niger), located 740 km east of Niamey (13.5214°N, 2.1053°E), between 28 Aug and 22 Sep 2006. The dots indicate the location of a dropsonde. From Drobinski et al. (2013).

end of August and end of September 2006 [for details on the technical aspect of the driftsondes and their operations see Drobinski et al. (2006, 2013)]. It was the first large deployment of driftsonde systems during a major field campaign. The driftsondes sampled squall lines in the troughs of AEW, the southeastern edge of the Tropical Storm (TS) Florence and Hurricanes Gordon and Helene. In addition to tracking potential hurricanes, the driftsondes gathered bird's-eye data on the Saharan air layer (SAL) over the Atlantic Ocean. The investigation of the cyclogenesis processes during the late stage of the monsoon was complemented by measurements collected from windsondes dropped from the National Aeronautics and Space Administration (NASA) DC-8 aircraft in the frame of the NASA-funded research program NASA-AMMA (NAMMA) (Zipser et al. 2009).

The focus of the present manuscript is to evaluate the analyses and forecast of the Météo-France [Action de Recherche Petite Echelle Grande Echelle (ARPEGE)] and ECMWF [Integrated Forecast System (IFS)] NWP models relative to different synoptic (e.g., AEW phases, mesoscale convective system life cycle, tropical cyclone genesis) and land surface (land and ocean) environments. The goal here is thus to use these data to identify the strengths and weaknesses of the models and to test the effectiveness of new developments in satellite data assimilation. One goal was to assimilate satellite-based advanced sounder data over land to improve the quality of moisture analysis in the tropics. Since the dropsonde data were not assimilated in real time, these measurements can serve as a tool for model evaluation, especially over areas such as Africa where very few in situ measurements are available (except for the specific case of the AMMA field campaign in 2006). It is not the first time that a study of this kind is conducted. For instance, Tompkins et al. (2005) use dropsonde measurements over the western Sahel region to evaluate the quality of the ECMWF analyses of the African easterly jet. These studies are necessary and must be renewed whenever possible to monitor changes in assimilation systems. The particularity of this study is to evaluate the analyses/forecasts from two NWP models in response to changes in data assimilation that can directly impact the hydrological cycle of the models. Other possible uses of campaign data can be done, including assimilation trials of these observations or their integration into a hybrid system, which may serve a wider community of scientists (Meynadier et al. 2010a).

Section 2 presents the driftsonde system. Section 3 details the synoptic environment associated with the various driftsonde flights. Section 4 provides a thorough evaluation of the NWP models described in section 2, and section 5 concludes the study.

2. Driftsonde observations

The drifting stratospheric balloons were developed by the Centre National d'Études Spatiales (CNES), whereas the dropsondes and gondola systems for their deployment were designed at the National Center for Atmospheric Research (NCAR) and their development was funded by the National Science Foundation and the National Oceanic and Atmospheric Administration. Each gondola held about 35 dropsondes designed by NCAR (the number of dropsondes could differ between the driftsondes) carried on the ballooning systems designed by CNES. The driftsonde was initially funded

in support of The Observing System Research and Predictability Experiment (THORPEX) program initiated under the World Meteorological Organization's (WMO) World Weather Research Program (e.g., Shapiro and Thorpe 2004) to accelerate improvements in NWP. Specifically, the intent was to obtain in situ observations in remote and oceanic regions where such measurements are difficult to obtain.

The Zinder site, located 740 km east of Niamey (13.5214°N, 2.1053°E), was selected to study the AEW that serve as seedlings for hurricanes during the late African monsoon period (August–September). During July–September 2006 period, a total of 27 AEWs (as compared with 31 in 2004 and 28 in 2005) were objectively analyzed using a method based on the wavelet analysis of the meridional wind field at 700 hPa, and moved across Africa into the Atlantic between about 10° and 20°N (Janicot et al. 2008). The large-scale AEWs activity has been quantified by computing the sum of the spectral density between 3- and 5-day periods as proposed by Lavaysse et al. (2006). July was very different from the later months, with six out of seven of the first waves forming close to the longitude of Niamey or west of it. In August, the AEWs were initiated farther east, between 10° and 20°E, but AEWs over Niamey were still weak. Starting at the end of August and going into September the AEWs became more coherent with stronger amplitudes over most of tropical North Africa. Interestingly, several AEWs also appeared to start farther east, between 20° and 30°E at this time. It should also be noted that all seven of the AEWs that became named tropical cyclones (Chris–AEW number 6; Ernesto–AEW number 13; Debby–AEW number 14; Florence–AEW number 18; Gordon–AEW number 19; Helene–AEW number 20; Isaac–AEW number 23; see Janicot et al. 2008) were initiated east of Niamey, and six of these occurred after the middle of August. After being launched from Zinder, each balloon drifted from Africa toward the Caribbean at heights of around 20 km, where light easterly winds prevailed. The trajectories exhibited cycloidlike patterns due to the presence of near-inertial waves (Hertzog et al. 2002) (Fig. 1). At least twice per day (0000 and 1200 UTC), each gondola released a dropsonde that fell by parachute. During its about 20-min descent, the sonde measured temperature and humidity with the position obtained using GPS. These positions were used to calculate the horizontal wind. The measurements were radioing data back to the gondola and then, by satellite, to the operation center in Paris, France. Whenever promising weather systems developed, the operation center signaled the gondola to release additional dropsondes as often as every 3 h. Eight driftsondes were released from Zinder during the late African monsoon period coinciding with the peak period for hurricane formation over the tropical Atlantic (August–September) and 124 sondes were successfully dropped from the eight driftsondes with 15 vertical profiles from the last dropsondes of driftsonde 8 sent to the global transmission system (GTS) for assimilation. However, the number of successfully dropped sondes differed between driftsondes. Table 1 summarizes the operation during the driftsonde deployment. During the driftsonde operations, between 29 August and 22 September 2006, seven AEWs have been detected (Janicot et al. 2008). Table 1 shows that the most successful flights corresponded to driftsondes 1, 3, 4, 5, 6, and 8. However, the synoptic environment documented with driftsonde 1 was not of high scientific interest and the driftsonde 8 trajectory was particularly complex and difficult to manage since the flight period corresponded to the weakening of the 50-hPa easterly winds due to a change of the Madden–Julian oscillation phase. So driftsonde 8 did not allow the tracking of any interesting meteorological event. In the following, we thus analyze in details the data collected with driftsondes 3–6, which documented in an unprecedented way AEW initiating continental mesoscale convective systems (MCS) evolving over the ocean into tropical storms like Florence and hurricanes like Gordon and Helene, some of them skirting the U.S. Atlantic and Gulf Coasts and all experiencing extratropical transition. Indeed, the strong added value of the driftsonde deployment during AMMA was the measurements of vertical profiles of

TABLE 1. Summary of driftsonde operations with the coordinates and date of the first and last dropsonde for each driftsonde, and the number of successful dropsondes.

Driftsonde no.	First dropsonde; last dropsonde	No. of successful dropsondes
1	(14.05°N, 6.04°E) 1406 UTC 28 Aug; (16.47°N, −44.03°E) 1217 UTC 2 Sep	8
2	(13.93°N, 8.13°E) 2118 UTC 29 Aug; (13.93°N, 8.13°E) 2118 UTC 29 Aug	1
3	(13.99°N, 7.04°E) 2351 UTC 1 Sep; (16.22°N, −58.07°E) 1312 UTC 9 Sep	33
4	(13.97°N, 8.14°E) 1942 UTC 4 Sep; (17.40°N, −55.14°E) 1110 UTC 11 Sep	14
5	(15.58°N, −10.07°E) 0807 UTC 9 Sep; (8.39°N, −50.09°E) 1808 UTC 13 Sep	25
6	(13.57°N, 8.00°E) 2055 UTC 9 Sep; (13.52°N, −46.03°E) 0005 UTC 18 Sep	26
7	(13.37°N, 7.03°E) 2358 UTC 12 Sep; (13.37°N, 7.03°E) 2358 UTC 12 Sep	1
8	(15.36°N, 6.10°E) 0603 UTC 16 Sep; (15.33°N, −15.07°E) 1742 UTC 22 Sep	16

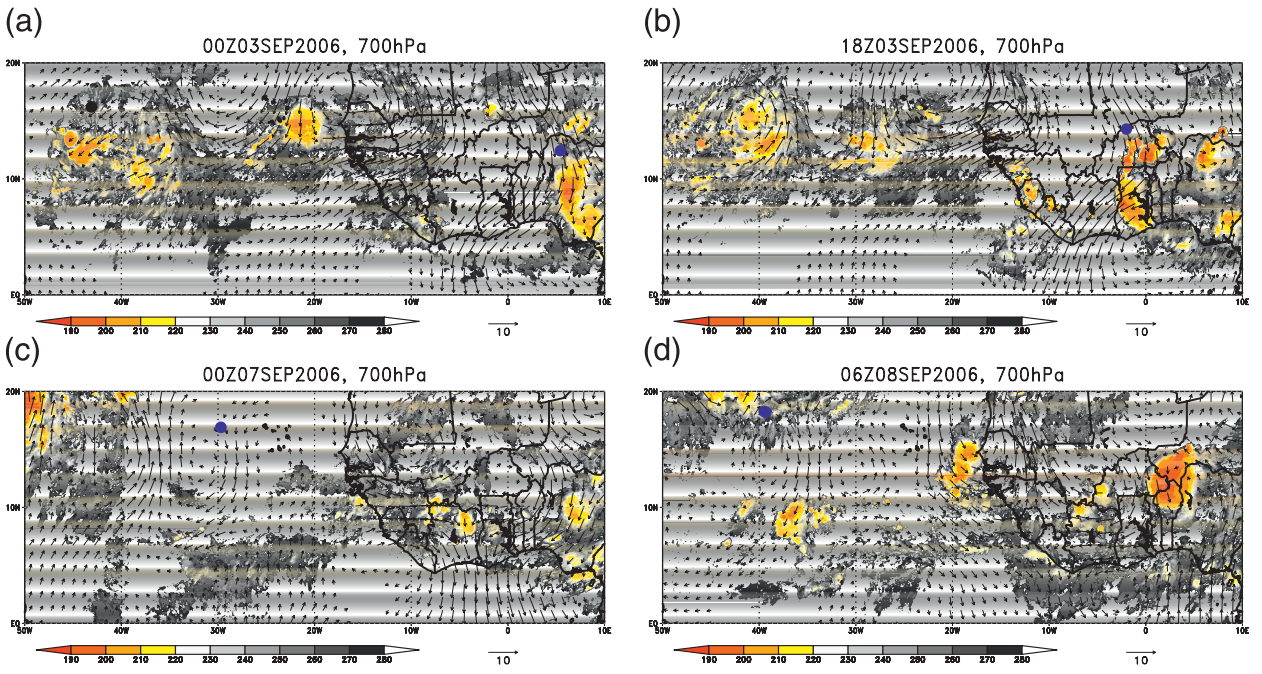

FIG. 2. MSG 10.8-μm channel brightness temperature (K) that indicates convective activity with superimposed 700-hPa wind field filtered over the 3–5 days shown with arrows (the absence of arrows indicates winds < 1 m s^{-1}) at (a) 0000 UTC 3 Sep 2006, (b) 1800 UTC 3 Sep 2006, (c) 0000 UTC 7 Sep 2006, and (d) 0600 UTC 8 Sep 2006. The black- and blue-filled dots indicate the locations of dropsondes from driftsondes 1 and 3, respectively. From Drobinski et al. (2013).

meteorological variables at high temporal resolution (every 6 h) and over the ocean where only very few measurements are available.

3. Driftsonde trajectories and synoptic environment

Figure 2 shows the Meteosat Second Generation (MSG) 10.8-μm channel brightness temperature that indicates convective activity, as well as the 700-hPa wind field filtered over the 3–5-day band that provides information on AEWs activity (Lavaysse et al. 2006) (see arrows; the absence of arrows indicates winds weaker than 1 m s^{-1}). It shows that driftsonde 3 is advected into the vicinity of an MCS propagating westward over the continent at about 15 m s^{-1}. At about 40°W, tropical depression Florence is forming (see Fig. 2b).

Figure 3 (first column) shows a time-versus-pressure[1] cross section of wind speed, temperature, and humidity constructed with the vertical profiles obtained by the sondes dropped from driftsonde 3. Figure 3 (second column) and Fig. 4 (first and second columns) are similar to Fig. 3 (first column), but for data obtained from the sondes dropped from driftsondes 4, 5, and 6, respectively. This set of figures gives us a global view of the vertical structure of the atmosphere as observed by dropsondes. It shows in particular that different weather regimes were observed during the drift of driftsondes. Note that driftsondes have drifted from their launch site to the ocean with dates of passage to the ocean on 4, 6, 9, and 12 September for driftsondes 3, 4, 5, and 6, respectively.

Figure 3a shows evidence of a strong wind tongue between 700 and 500 hPa corresponding to the AEJ (between 4 and 5 km). Figure 3e shows the moist African planetary boundary layer between 2 September and 5 (75% relative humidity) extending up to about 850 hPa (about 1-km height). Above the planetary boundary layer, layers of saturated air up to 500 hPa (i.e., 5 km) reveal the proximity of the convective activity.

On 7 September, dropsondes are released from driftsonde 3 a few hundred kilometers downstream of Florence, located at about 50°W, which in the meantime had been classified as a tropical storm (it becomes a hurricane on 10 September 2006). The near-surface wind decreases in the disturbed environment near

[1] For comparison convenience, the vertical coordinate is in pressure levels (hPa) since it is the commonly used coordinate of NWP models. Since there were no pressure measurements on the dropsondes during AMMA, the height-to-pressure level conversion is provided by the NWP models. However, because of the absence of pressure measurements, only relative humidity is shown in this article as a humidity measurement from both dropsondes and NWP models.

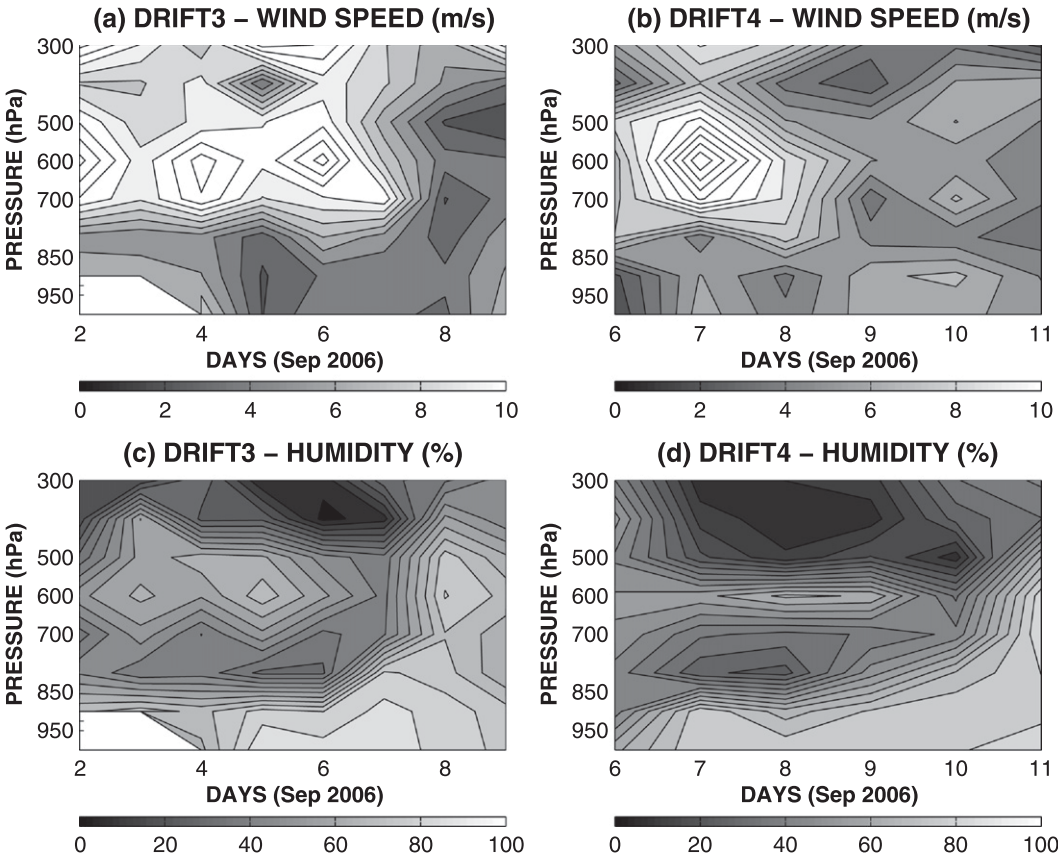

FIG. 3. Time-vs-pressure cross section of (a),(b) wind speed and (c),(d) humidity constructed with the vertical profiles obtained by (left) driftsonde 3 (blue trajectory in Fig. 1) and (right) driftsonde 4 (yellow trajectory in Fig. 1). The contour interval is 2.3% for humidity and 0.45 m s^{-1} for wind speed. Note that driftsondes have drifted from their launch site to the ocean with dates of ocean passage of 4 and 6 Sep for driftsondes 3 and 4, respectively.

Tropical Storm Florence as shown in Fig. 3a, while the planetary boundary layer humidity and depth increase (up to about 90% relative humidity and up to 700 hPa, i.e., 3 km on 7 September) before reaching the disturbed environment near Florence where very intense convection occurs (Fig. 3e). Figure 3b is similar to Fig. 3a for driftsonde 4. However, the much lower number of successful dropsondes does not allow the documentation of finescale structures over the Atlantic Ocean. It, however, shows a disturbed environment similar to driftsonde 3 less than 200 km south of the developing Tropical Storm Gordon at about 55°W (not shown) on 11 September with large humidity extending up to the tropopause and weak near-surface winds. The existence of weak surface winds is surprising since one may associate naturally developing tropical storms with large evaporation and thus strong winds. The vertical profiles of relative humidity documented by the dropsondes of driftsonde 4 around 7 September also show evidence of very low humidity values just above the planetary boundary layer (around 20% relative humidity) and at about 500 hPa, that is, 5–6-km height (below 10% relative humidity) corresponding to the AEJ (Fig. 3). The low-level dry layer was identified as a strong dry air outflow from the Sahara by the *Meteosat-8/Geostationary Operational Environmental Satellite-10 (GOES-10)* combined Saharan air layer product (Fig. 5). The very dry air conveyed by the AEJ originated in the upper levels (200–250 hPa) on the anticyclonic side of the polar jet stream at 50°N as diagnosed by the method proposed by Roca et al. (2005).

Figure 6 is similar to Fig. 2 between 11 and 17 September. Driftsonde 5 (purple dots) observed the atmosphere ahead (to the east) of Tropical Storm Helene, which initiates on 1800 UTC 11 September at over the coast of Senegal and moves westward at a propagation speed of about 8 m s^{-1}. Driftsonde 6 (green dots) observed the atmosphere downstream (to the west) of Tropical Storm Helene. Figure 4 shows that after the

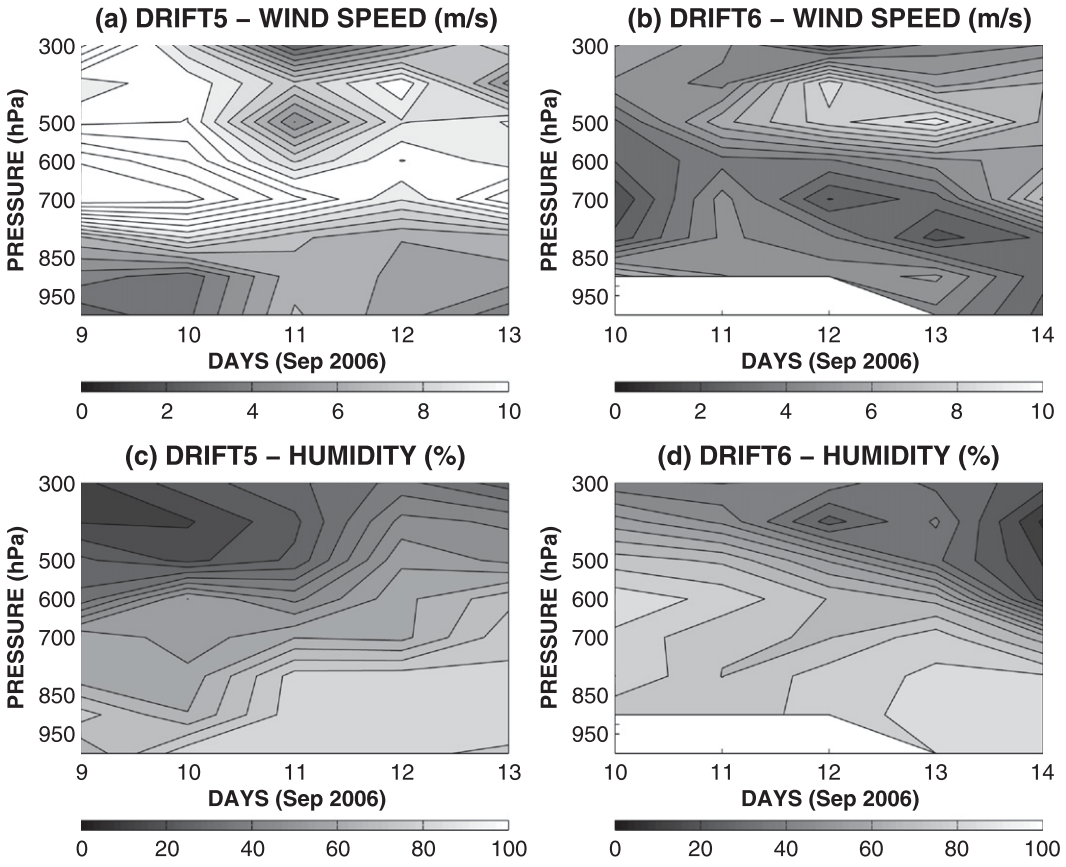

FIG. 4. As in Fig. 3, but for the sondes dropped from driftsonde 5 (purple trajectory in Fig. 1) and driftsonde 6 (green trajectory in Fig. 1) with ocean passage dates of 9 and 12 Sep for driftsondes 5 and 6, respectively.

formation of three successive storms in about two weeks, all of which evolved into hurricane category, driftsondes 5 and 6 probe a much more disturbed environment than for Florence, with higher convective activity both over the continent and the ocean with nearly saturated air observed up to 5 km along the driftsonde tracks. The AEJ tends to weaken during driftsonde-6 flight.

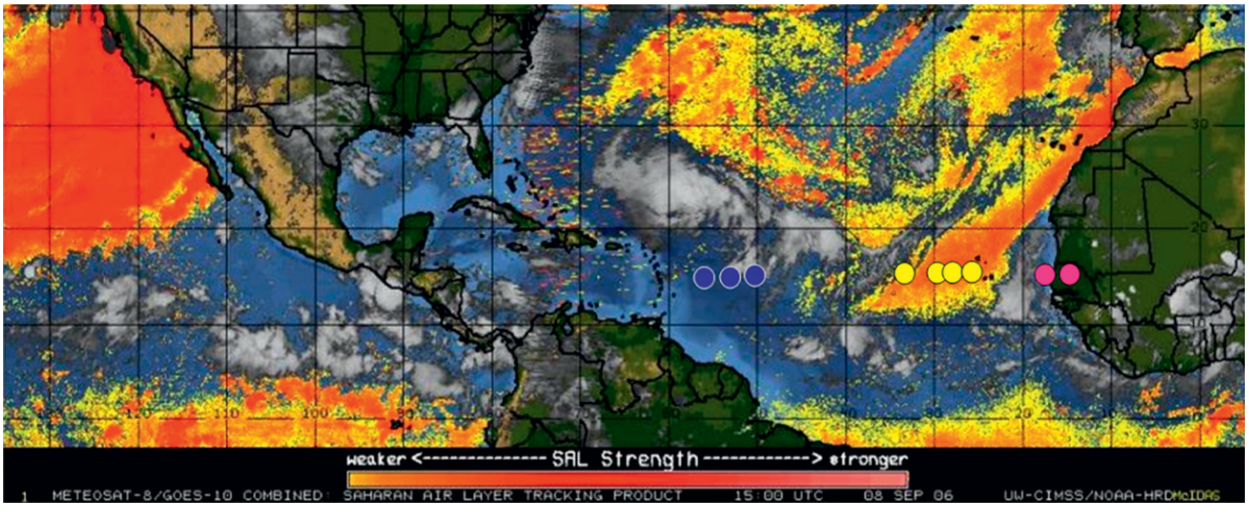

FIG. 5. *Meteosat-8/GOES-10* combined Saharan air layer product at 1500 UTC 8 Sep 2006. The blue-, yellow-, and pink-filled dots correspond to dropsondes launched in the vicinity of the SAL from driftsondes 3, 4, and 5, respectively.

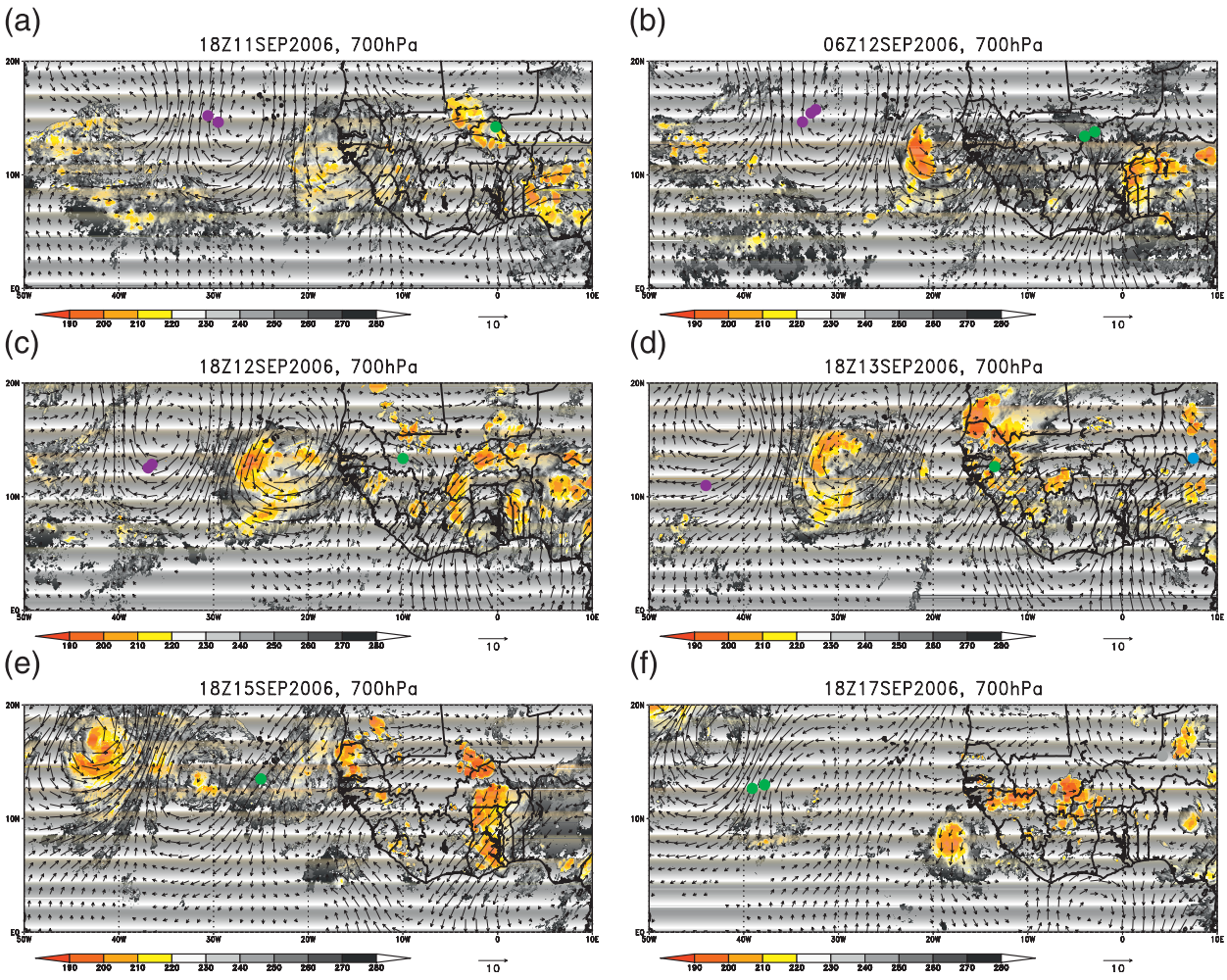

FIG. 6. As in Fig. 2, but for (a) 1800 UTC 11 Sep, (b) 0600 UTC 12 Sep, (c) 1800 UTC 12 Sep, (d) 1800 UTC 13 Sep, (e) 1800 UTC 15 Sep, and (f) 1800 UTC 17 Sep. The purple-, green-, and cyan-filled dots indicate the locations of dropsondes from driftsondes 5, 6, and 7, respectively. From Drobinski et al. (2013).

4. Evaluation of atmospheric analyses

a. Assimilation experiments during summer 2006

In this work, the atmospheric analyses and forecasts from two four-dimensional variational data assimilation (4D-Var) systems are compared with observations of dropsondes to assess the strengths and weaknesses of the models. The IFS and the ARPEGE 4D-Var systems are considered for the comparison. A 4D-Var system seeks an optimal state of the atmosphere, over a window of 6 h for ARPEGE and 12 h for IFS, consistent with all available observations and with information from the past (short-range forecasts). This translates into finding an optimal trajectory of the model, within the assimilation window, which represents the best compromise between observations and background information. The optimal state of the atmosphere is obtained by minimizing a cost function given the distance of the model trajectory to the observation and to the background. To get the analysis, IFS and ARPEGE use the so-called incremental approach to correct iteratively the initial condition (Rabier et al. 2000; Courtier et al. 1994; Veersé and Thépaut 1998).

In the context of the AMMA project, assimilation experiments making use of a larger number of Medium Resolution Imaging Spectrometer (MERIS) and Advanced Microwave Sounding Unit A and B (AMSU-A/B) data over land were considered better than control experiments with regard to the quality of their analyses and forecasts. The key result was to improve the quality of moisture analysis in the tropics. These results are particularly relevant for areas such as tropical continental regions for which the in situ observation network is fairly sparse. Besides improving the forecast skills, assimilating

TABLE 2. Assimilation experiments.

Expt	System	Version	Description
IFS-CTL	IFS	CY35R1	Operational configuration
IFS-EXP	IFS	CY35R1	IFS-CTL + assimilation of low-level temperature and humidity observations from AMSU-A/-B over land
ARP32-CTL	ARPEGE	CY32T0	Operational configuration
ARP32-EXP	ARPEGE	CY32T0	ARP32-CTL + assimilation of low-level temperature and humidity observations from AMSU-A/-B over land
ARP33-CTL	ARPEGE	CY33T1	Operational configuration
ARP33-EXP	ARPEGE	CY33T1	ARP33-CTL + assimilation of low-level temperature and humidity observations from AMSU-A/-B over land

many more satellite data over land brings significant changes to atmospheric fields from the analysis (humidity, temperature, and wind).

Table 2 summarizes the characteristics of assimilation experiments that will be discussed in this article. The experiments are distinguished from each other through the system version (CY33T1 for ARPEGE and CY35R2 for IFS) and the satellite data used during assimilation. Indeed, some experiments are representative of the operational models whereas other experiments take advantage of recent developments in satellite radiance assimilation. Indeed, better modeling of land surface emissivity at microwave frequencies, has made possible the assimilation of observations sensitive to low atmospheric layers and to the surface (Karbou et al. 2006). This approach was developed in ARPEGE and was later extended to the IFS system (Karbou et al. 2007; Krzeminski et al. 2008). Bauer (2009) used TCWV from MERIS observations to constrain the humidity analyses over land. ARPEGE experiments studied here are different from those studied in Karbou et al. (2010) because they are based on two different ARPEGE cycle versions (CY33T1 against CY32T0). CY32T0 was operational between 5 September 2007 and 6 February 2008 whereas the ARPEGE CY33T1 was operational between 22 September 2009 and 6 April 2010. Version CY33T1 brings important changes in the physics package including an updated turbulence scheme (Cuxart et al. 2000) and a mass flux convection scheme (Bechtold et al. 2001). The changes in physics have led to a more realistic representation of humidity, clouds and convection at the low levels. Figure 7 shows the average TCWV differences over 45 days (from 1 August to 14 September 2006) for ARP32-EXP − ARP32-CTL and ARP33-EXP − ARP33-CTL.

The humidity dipole over West Africa, which has already been analyzed with CY32T0 experiments (Karbou et al. 2010), highlights a humidity bias in the model (Fig. 7a). The bias is weakened by switching to the CY33T1 version of the ARPEGE model (Fig. 7b). The shape of the humidity dipole remains unchanged but the intensity of the bias is reduced. A similar humidity bias has also been observed when TCWV from MERIS observations were assimilated in IFS (Bauer 2009). However, these remarks are not sufficient to identify the best assimilation experiment whose outputs are closer to reality, and a comparison with independent data is needed. Given the availability of GPS data during the AMMA campaign (Bock et al. 2007), a first evaluation of the ARPEGE model was performed and was found in favor of the experiment making use of additional satellite data sensitive to moisture over land (Karbou et al. 2010).

There is a need for independent and reliable data that could be used to evaluate any changes in the models. In data assimilation there are several methods that are useful for evaluating the models but use data already assimilated in the system such as the fit to observations. Figure 8a shows the model fit in terms of root-mean-square (RMS) errors to radiosonde meridional wind observations over West Africa (5°–20°N, 20°W–10°E) with the ARPEGE model based on the CY33T1 and CY32T0 cycles (ARP32-CTL and ARP33-CTL, respectively; Table 2). Figure 8b is similar to Fig. 8a with dropsonde meridional wind observations over land.

The RMS with CY33T1 cycle is significantly smaller than with CY32T0 cycle with approximately the same number of assimilated radiosondes. The relative improvement of the RMS is about 10% in the vertical. The effect of the addition of microwave surface sensitive observations over land has also been quantified (ARP32-EXP and ARP33-EXP; Table 2). The fit is often better for the experiments assimilating more observations over land especially in the low levels. There is a net benefit with CY33T1 cycle, except around 400 hPa where there is a deterioration of statistics compared to CY32T0 (not shown). Similar conclusions can be drawn for other types of assimilated observations (not shown). This type of diagnosis allows the verification of the

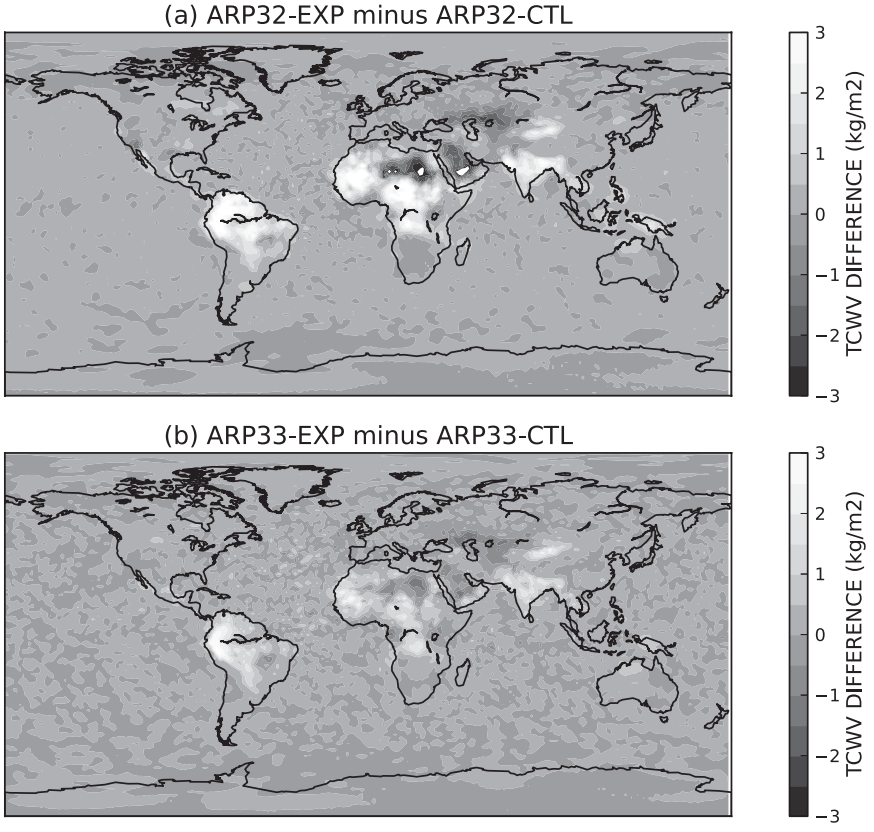

FIG. 7. Average TCWV differences over 45 days (1 Aug–14 Sep 2006): (a) ARP32-EXP − ARP32-CTL and (b) ARP33-EXP − ARP33-CTL. Negative (positive) values indicate that the control assimilation is moister (drier) than in ARPEGE-EXP.

proper consistency of the assimilation (analysis closer to the baseline observations) but remains questionable because the comparisons are made with data that are assimilated.

Dropsondes are a complementary source of independent measurements for assessing the quality of model outputs in the vertical. These data were not assimilated and can therefore serve as a tool for model evaluation

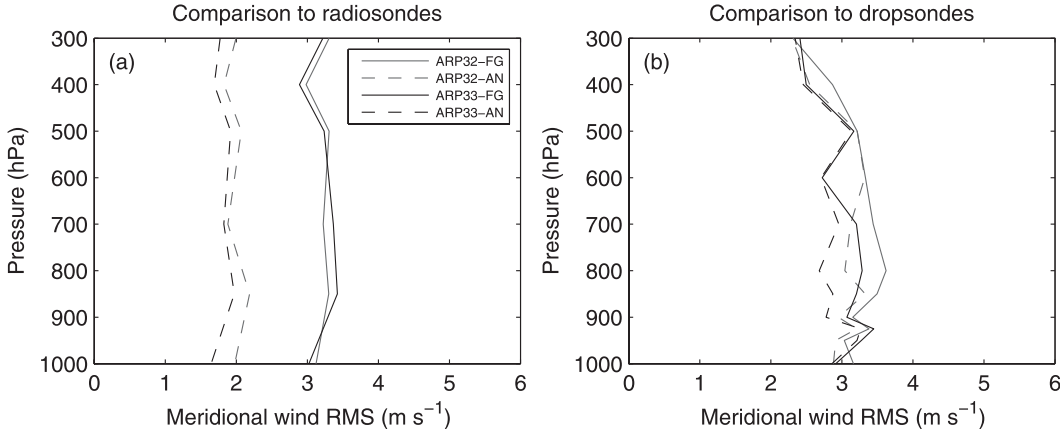

FIG. 8. RMS errors of the background (observed − 6-h forecast) (solid), and of the analysis (observed − analysis) (dashed) for departures of (a) the assimilated radiosonde meridional wind observations and (b) nonassimilated dropsonde meridional wind observations over West Africa for ARPEGE-CY32T0 and ARPEGE-CY33T1. The period is 1–14 Sep 2006.

TABLE 3. Total number of dropsonde observations used for comparison with IFS and ARPEGE analyses. Statistics are presented as a function of pressure level for land, sea, SAL, and TS environments.

Pressure (hPa)	Land	Sea	SAL	TS
1000	6	55	2	14
950	23	57	2	14
925	23	57	2	14
900	23	57	2	14
850	23	57	2	14
800	23	57	2	14
700	23	57	2	14
600	22	57	2	14
500	22	57	2	14
400	22	57	2	14

especially over areas such as Africa where very few in situ measurements are available. There are some similarities between the RMS errors relative to radiosondes and to dropsondes (Fig. 8). The comparison is made with different data but for the same geographical area. If the shape of the RMS curves is similar, the RMS values relative to dropsondes are higher than those relative to radiosondes, even though one has to keep in mind that the number of radiosonde data used to estimate the RMS errors is much higher than the number of dropsondes. As expected RMS errors in the analyses are lower than in the 6-h forecasts and in particular for CY33T1 cycle; this is especially true above 900 hPa. However, the decrease of RMS errors in the analysis when compared with a short-range forecast in Fig. 8b is less evident than in Fig. 8a.

b. Contribution of land observations in ARPEGE

Since all diagnostics are better with CY33T1 cycle, the ARPEGE model assessment is made with the CY33T1 cycle. Vertical profiles of temperature, humidity, and zonal and meridional wind speed from ARP33-CTL and ARP33-EXP analyses and forecasts (1.5° resolution at standard pressure levels) are compared with available dropsondes and comparisons are performed for various surface types (land, sea) and environment (SAL and TS). The vertical resolution of the dropsonde vertical profiles is typically about 10 m so there is no data interpolation when comparing the measured profiles with the NWP models. Conversely, regarding the vertical profiles computed from the NWP model simulations, we have taken the closest profiles to the time of dropsonde observations and we averaged the four model outputs surrounding the dropsonde observation location. For a given pressure level, we have selected the closest dropsonde measurement the standard level.

TABLE 4. Temperature, relative humidity, zonal, and meridional wind statistics with respect to dropsonde data (mean, standard deviation of analysis minus dropsonde) over land: ARP33-CTL and ARP33-EXP analyses are collocated with dropsondes.

Parameter	Pressure level (hPa)	Bias CTL/EXP	Std CTL/EXP
T (K)	1000	1.63/1.34	3.12/3.13
	950	0.15/−0.12	2.26/2.29
	925	0.23/−0.06	2.06/2.02
	900	0.37/0.09	1.83/1.74
	850	0.38/0.41	2.08/2.11
	800	0.12/0.14	2.33/2.38
	700	0.04/0.22	1.95/1.93
	600	−0.10/−0.19	1.64/1.58
	500	−0.67/−0.66	1.19/1.20
	400	−0.99/−0.98	1.07/1.08
RH (%)	1000	−7.91/−5.51	6.72/5.42
	950	2.24/4.68	11.15/9.38
	925	1.02/3.73	12.53/11.36
	900	−0.07/3.00	13.94/12.34
	850	3.12/3.83	11.47/13.52
	800	3.01/3.88	12.53/15.10
	700	2.43/−1.20	17.27/15.81
	600	−5.89/−2.65	20.81/15.41
	500	−7.66/−3.60	17.07/17.06
	400	−1.10/−1.85	17.15/15.66
U (m s^{-1})	1000	1.23/1.00	2.54/2.57
	950	1.05/0.93	2.86/2.84
	925	1.05/0.77	2.80/2.93
	900	0.68/0.35	3.30/3.42
	850	0.77/0.51	3.36/3.33
	800	0.33/0.46	3.07/3.01
	700	−0.48/−0.30	2.43/2.46
	600	−0.15/−0.27	2.10/2.22
	500	−0.98/−0.99	3.40/3.61
	400	0.09/−0.16	2.95/2.86
V (m s^{-1})	1000	1.34/0.84	2.65/2.73
	950	0.04/−0.30	3.11/3.20
	925	0.16/−0.08	3.12/3.26
	900	0.52/0.41	2.63/2.75
	850	0.32/0.39	3.01/2.85
	800	−0.12/0.14	2.75/2.68
	700	0.03/0.24	3.02/2.95
	600	1.14/1.22	2.52/2.42
	500	1.41/1.32	3.09/2.84
	400	−0.17/0.10	2.24/2.45

Table 3 shows the total number of dropsonde observations used in the comparison for the different types of investigated environment.

Table 4 compares average values of meteorological fields (temperature, humidity, zonal wind, and meridional wind) from ARP33-CTL and ARP33-EXP analyses with dropsonde profiles over land. It quantifies the comparison in terms of mean and standard deviation with respect to dropsondes (analysis minus dropsonde). The dropsonde profile is fairly well represented in ARP33-EXP. In particular, the temperature bias is significantly improved, especially below 850 hPa, probably

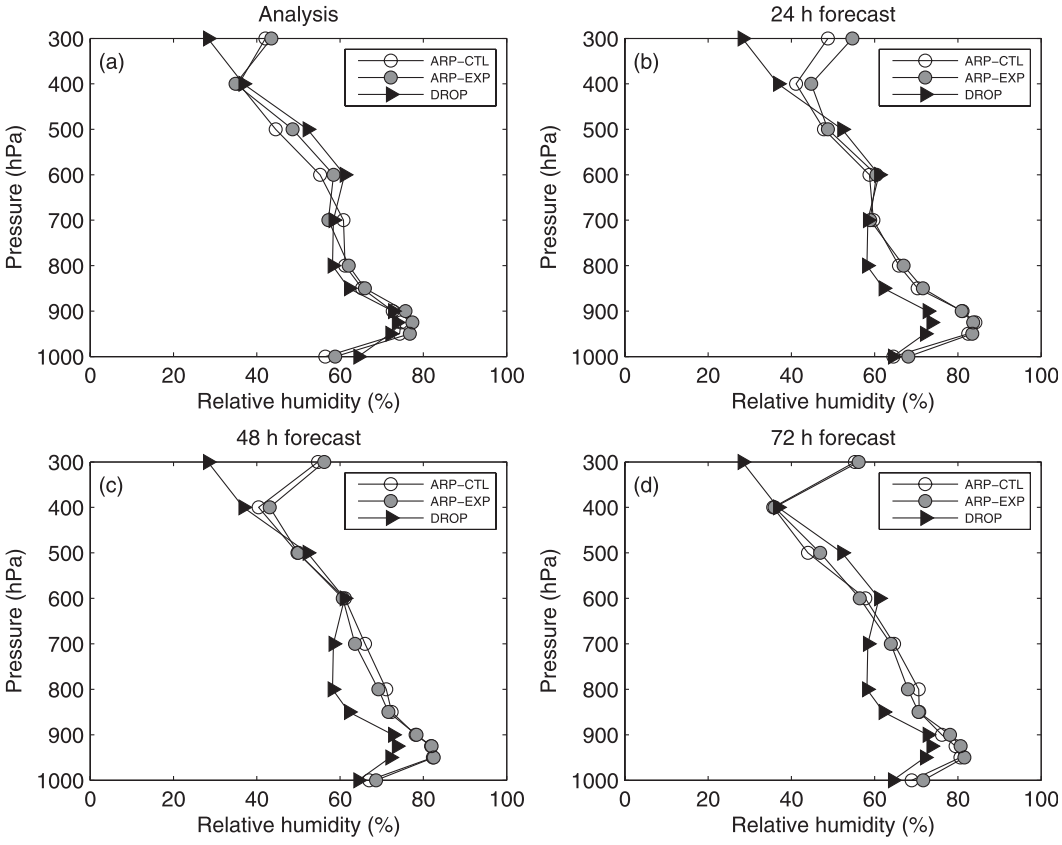

FIG. 9. Vertical profiles of relative humidity of ARP33-EXP and ARP33-CTL collocated with dropsondes over land using (a) analyses and (b) 24-, (c) 48-, and (d) 72-h forecasts.

because of the assimilation of AMSU-A observations that are sensitive to temperature at lower levels. The bias is −0.09 K around 950–925 hPa while it is close to 0.19 K in the ARP33-CTL. The values of standard deviation at these levels remain similar between ARP33-EXP and ARP33-CTL. At surface level, the temperature bias reduces from 1.63 to 1.34 K. The moisture profile of ARP33-EXP is also closer to the dropsondes particularly near the surface and above 700 hPa. Moisture is, however, overestimated around 900 hPa. For the zonal wind component, ARP33-EXP performs better than ARP33-CTL in the vertical. For the meridional wind, ARP33-EXP generally reduces its bias in the low levels (from 1.34 to 0.84 m s^{-1} at 1000 hPa) and shows smaller standard deviations. To summarize, we can say that, when compared with ARP33-CTL, ARP33-EXP displays improved statistics, especially in the lower atmospheric layers, with respect to dropsonde data.

The analyses are in much better agreement with dropsondes than short-range forecasts. Figure 9 shows vertical profiles over land of humidity from dropsondes, analyses, 24-h forecasts, 48-h forecasts, and 72-h forecasts using ARP33-EXP and ARP33-CTL. The moisture in the lower layers is overestimated regardless of the forecast range. Above 600 hPa, the agreement remains within 10% until the 48-h forecast, especially for ARP33-EXP. Similar results were found by examining temperature and the two wind components (not shown). For temperature, the deterioration is even visible in the 24-h forecast for both ARP33-CTL and ARP33-EXP. The statistics improve in the 72-h forecast for moisture, but also for temperature. It is consistent with previous results showing a positive impact of microwave observations at longer forecast ranges (Karbou et al. 2007, 2010).

Over the sea, very little difference is found between ARP33-CTL and ARP33-EXP analyses and forecasts, as for instance shown with moisture profile (Fig. 10) (detailed statistics on the temperature, humidity, and wind over sea are not shown).

Despite the improvements brought by the assimilation of new observations, some concerns remain and this invites further work on physics and other assimilation related issues. Evaluation of experiments with dropsondes confirmed some previous findings and highlighted new challenges especially related to the representation of wind.

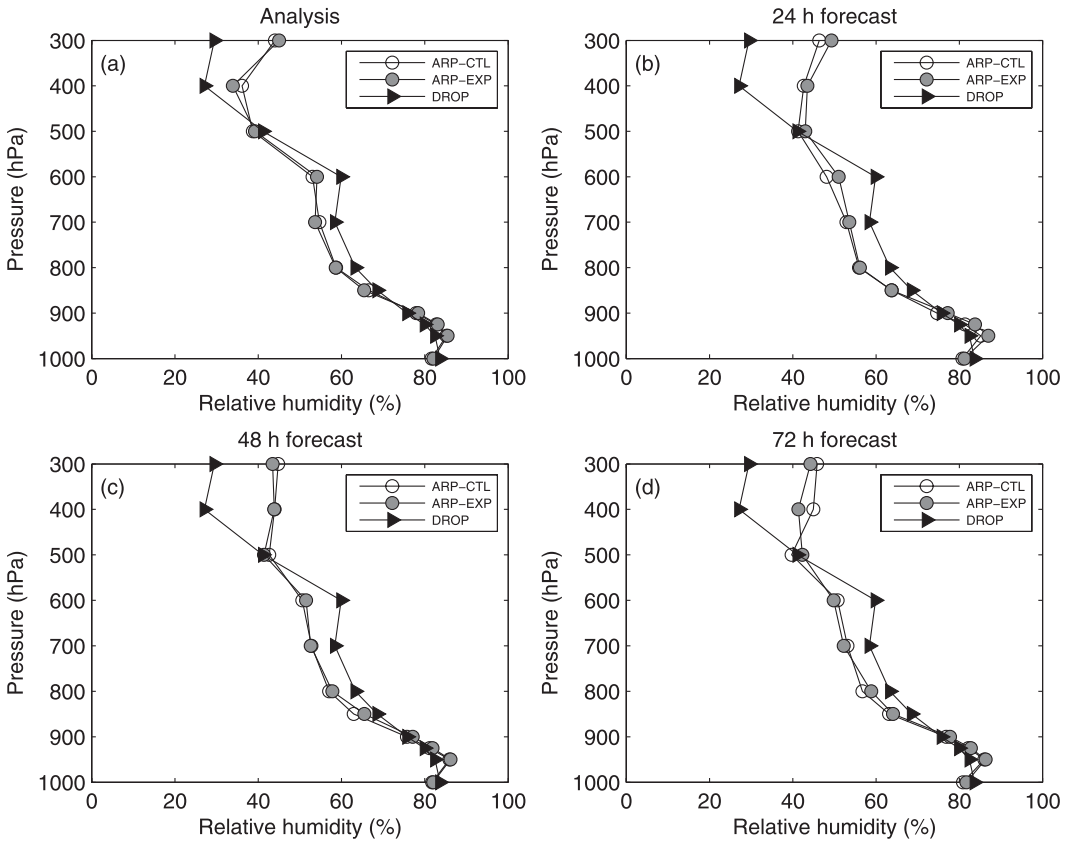

FIG. 10. As in Fig. 9, but over the sea.

c. *Comparison with IFS and ARPEGE*

In what follows, we carry out the evaluation of ARPEGE and IFS using dropsonde data from the ARP33-EXP and IFS-EXP experiments (Table 2). The choice of the most recent cycles that assimilate more observations over land surfaces, offers the best performance in terms of analyses and forecasts. Figure 11 (or Fig. 12) and Fig. 13 (Fig. 14) are similar to Fig. 3 (Fig. 4) for ARPEGE and IFS analyses, respectively.

A surprisingly good agreement is found between measurements and ARP33-EXP and IFS-EXP analyses. Considering driftsonde 3, the two models succeed in simulating the AEJ with winds up to 13–15 m s^{-1} around 700 hPa until 7 September and a humid planetary boundary layer below the AEJ (70% relative humidity). In the vicinity of Tropical Storm Florence, they reproduce accurately the weak near-surface winds and the quasi-saturated air (80% relative humidity). There is also a good agreement between the simulated and observed temperature field over the driftsonde-3 trajectory. As mentioned earlier, measurements from driftsonde 4 show the occurrence of two zones of very dry air just above the African planetary boundary layer at around 5–6-km height. IFS and ARPEGE models are also able to reproduce the two distinct dry air masses with relative humidity as low as 20%–10%, but IFS performs better in separating the two distinct dry air masses. At the beginning of the driftsonde-4 observation period, the models are again able to simulate the AEJ. We note an underestimation of the temperature near the surface associated with saturated air in both models (from −2 to −4 K; see possible explanation herein) and an overestimation in ARPEGE at around 600 hPa, located between the two very dry air masses. We can therefore say that the models tend to underestimate the temperature within moist air and to overestimate it within dry air. No significant temperature bias is observed when comparing ARP33-EXP and IFS-EXP analyses with driftsonde-5 measurements, while for driftsonde 6 the models overestimate temperature near 600–700 hPa around 11 September, when and where the measurements show weak winds and very moist air.

The present comparison with dropsondes aims at discussing the accuracy of the analysis and forecast to reproduce the vertical structure of the atmosphere. We

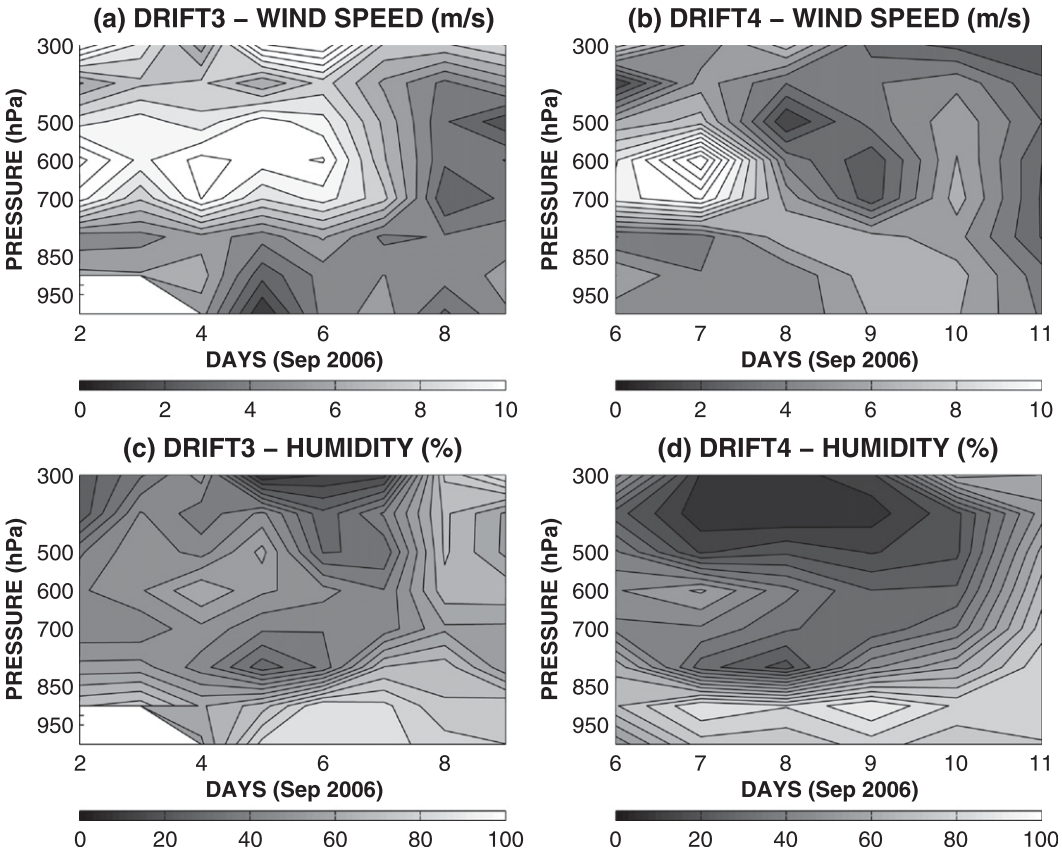

FIG. 11. As in Fig. 3, but for ARPEGE analyses collocated with dropsondes.

now perform conditional analysis regarding the surface type (land or sea) and atmospheric situations of interest, that is, SAL and TS environments. Indeed, as mentioned previously, the SAL and AEWs interact in complex ways and play a role not well understood in the evolution of tropical cyclones. Karyampudi and Carlson (1988) and Karyampudi and Pierce (2002) suggest a potential positive influence on the growth of easterly waves and tropical cyclones in the Atlantic, whereas Dunion and Velden (2004) describe several potentially negative influences of the SAL. Finally, Braun (2010) suggests that the SAL is not a determinant of whether a storm will intensify or weaken in the days after formation.

1) EVALUATION OVER LAND AND SEA

Figure 15 shows vertical profiles over land and sea of humidity, temperature differences, and zonal and meridional winds from ARP33-EXP and IFS-EXP analyses collocated with the dropsondes' data. Figures 15a and 15b show that IFS and ARPEGE models reproduce very well the shape of the vertical structure of moisture although with differences compared to observed values of the dropsondes. There is a tendency to overestimate moisture in the lower layers over both land and sea in particular for ARPEGE (about −5%). The bias with respect to dropsonde measurements is about +4% and +0.2% at 950 hPa and about −1.2% and +0.4% at 700 hPa for ARPEGE and IFS, respectively.

For temperature over land, Figs. 15c and 15d show that the IFS model is less biased near the surface in comparison with ARPEGE (0.09 vs 1.34 K). This bias is even more pronounced when using ARP33-CTL, as shown in the previous section. The ARPEGE temperature bias is smaller at 800–900 hPa, while it is larger for IFS at these pressure levels (+0.4 vs −0.6 K). Moreover, IFS is more biased near the sea surface with a mean bias of −0.7 K, while ARPEGE displays no significant bias. IFS and ARPEGE models reproduce very well the zonal wind both over land and sea with a slight difference of the near-surface wind over land by +1 m s^{-1} (i.e., about 20% error) (Figs. 15e,f). The meridional wind is less accurately simulated with a difference from +1 to 1.5 m s^{-1} over land (i.e., about 100% error) and from −0.5 to −1 m s^{-1} over sea (i.e., about 100% error) (Figs. 15g,h), thus producing different wind directions. One can, however, note the differential behavior of

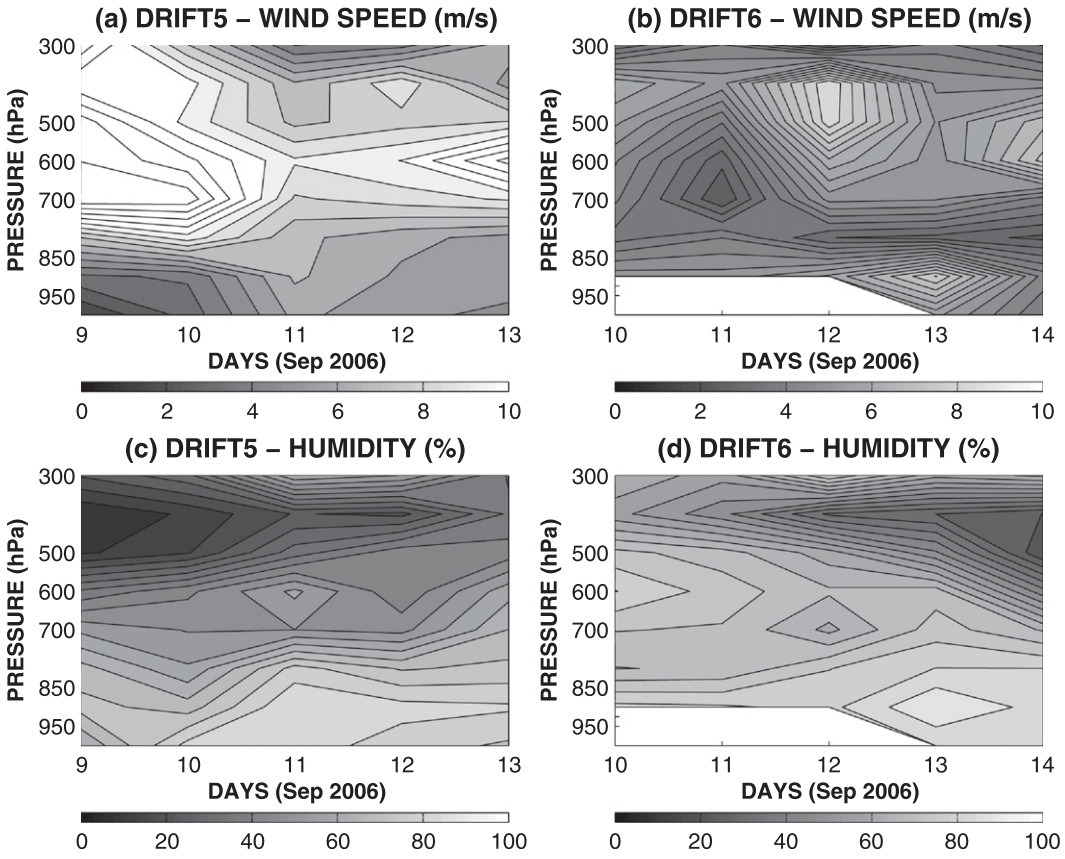

FIG. 12. As in Fig. 4, but for ARPEGE analyses collocated with dropsondes.

both models depending on the surface type: IFS is closer to the dropsondes over land above 800 hPa while ARPEGE is closer to the dropsondes below 800 hPa. Over sea, the two models almost coincide.

2) EVALUATION IN SAL AND TS ENVIRONMENTS

Figure 16 shows vertical profiles of humidity, temperature differences, and zonal and meridional winds from ARP33-EXP and IFS-EXP within SAL and in the vicinity of TS. The number of profiles within the SAL is small (two successful dropsondes), which reduces the present result's significance. However, SAL situations are rarely observed and even with a reduced number of profiles we strongly believe it is worth the investigation. A good surprise is that ARP33-EXP and IFS-EXP analyses accurately reproduce the vertical structure of moisture within the SAL. This may be due to a weak heating of the atmosphere by the dust layer, which thus may not change the static stability of the atmosphere. Indeed, when the radiative effect of dust is large, a better prediction of thermodynamical profiles and precipitation is obtained when a dust prognostic scheme is used rather than climatology or when dust effects were ignored (Chaboureau et al. 2011). Two maxima of humidity (near the surface and at around 600 hPa) are present in ARP33-EXP and IFS-EXP in agreement with the dropsondes. IFS better reproduces the second humidity maximum than ARPEGE. Similarly, two moisture minima are also present in ARP33-EXP and IFS-EXP, at around 850 hPa (20% relative humidity) and at 500 hPa (about 10% relative humidity). However, ARP33-EXP and IFS-EXP both have a cold temperature bias that is maximum around 900 hPa (Figs. 16c,d). It is difficult at this time to identify the cause of this cold bias but a possible explanation for such a consistent behavior between ARP33-EXP and IFS-EXP is the absence of aerosol representation in the two models. The SAL surge transports an optically deep aerosol load over the Atlantic. Studies conducted in the framework of AMMA have shown evidence of significant heating associated with dust transport in West Africa (Lemaître et al. 2010; Lavaysse et al. 2011) due to the aerosol semidirect effect. Indeed, the heating rate is proportional to the irradiance divergence. The negative surface forcing of the aerosols causes an overall decrease in the surface temperature below the dust layer. In contrast, there is

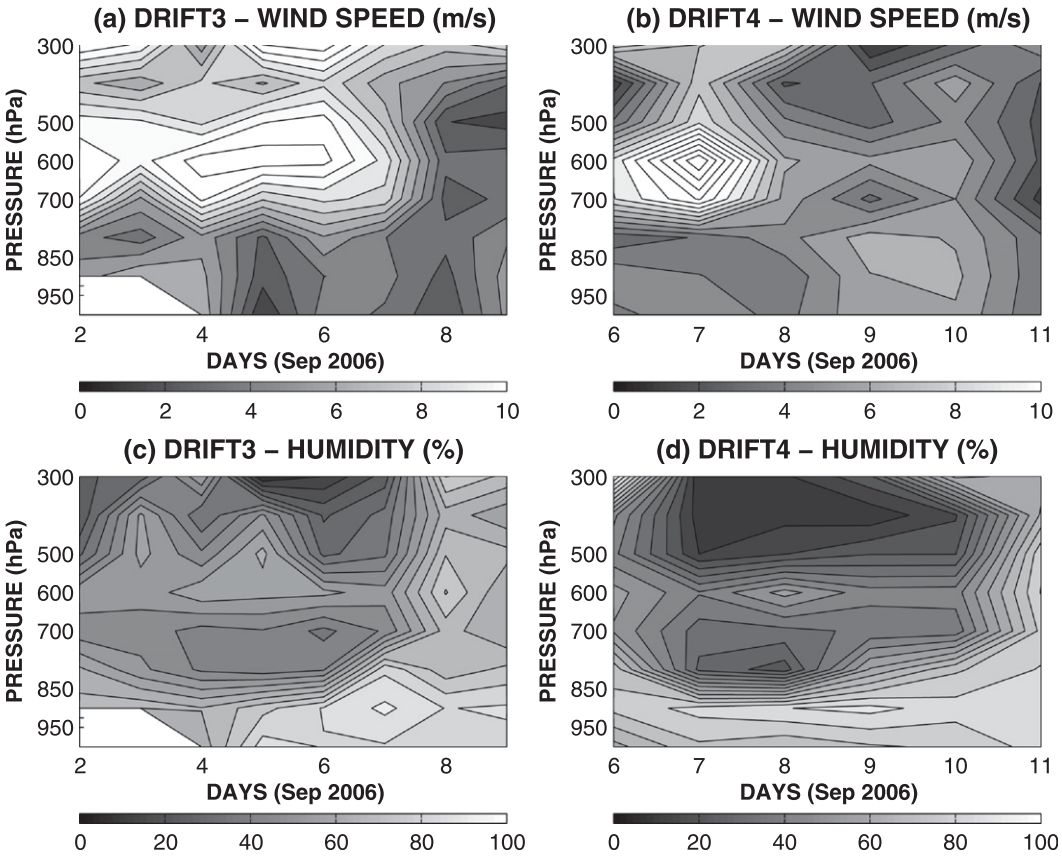

FIG. 13. As in Fig. 3, but for IFS analyses collocated with dropsondes.

a gain of radiative energy in the atmospheric column attributed to absorbed incident solar radiation within the dust layer. The effect is reflected in the 900-hPa temperature fields, which are underestimated by the models because the aerosol effect is absent. The main daytime effect of mineral dust is to redistribute radiative heating from the surface to the atmosphere and to stabilize the atmospheric stratification. Indeed, Solmon et al. (2008) have evidenced dust surface cooling as well as an elevated heat pump effect in the higher troposphere induced by the dust diabatic warming. In our case, daytime heating rates are on average between 1.5 and 4 K day^{-1} but can reach values as high as 8 K day^{-1}. The absence of aerosol radiative feedback on the temperature field might thus explain the from −2 to −4 K cold temperature bias in the two models. However, this needs a dedicated study, which is left for future work. Figures 16e and 16f show that ARP33-EXP and IFS-EXP produce differences from −3 to −4 m s^{-1} for the easterly zonal wind above 900 hPa and about +1 m s^{-1} for the zonal wind below 900 hPa. Figures 16g and 16h show that both ARPEGE and IFS models fail in reproducing the vertical structure of the meridional wind above 800 hPa (2–3 m s^{-1} difference). Below this level, ARPEGE provides maximum wind at the correct pressure level but not with the right intensity while IFS provides maximum wind with good intensity but not at the right pressure level (except at the surface level where there is a rather good agreement).

For a TS environment, moisture retrievals from ARP33-EXP and IFS-EXP are in very good agreement with dropsondes, especially ARP33-EXP, which displays very small biases with respect to the measurements. A similar comment can be made for temperature. This is less the case for the zonal wind for which IFS reproduces quite well its vertical structure. Finally, both models underestimate the meridional wind component.

5. Conclusions

In this paper, we conducted a comparative study between dropsonde observations and the outputs of two NWP models (IFS and ARPEGE). The purpose of the study is to assess, as independently as possible, the performance of both models over a region with very sparse observations. Note that the assimilation experiments that

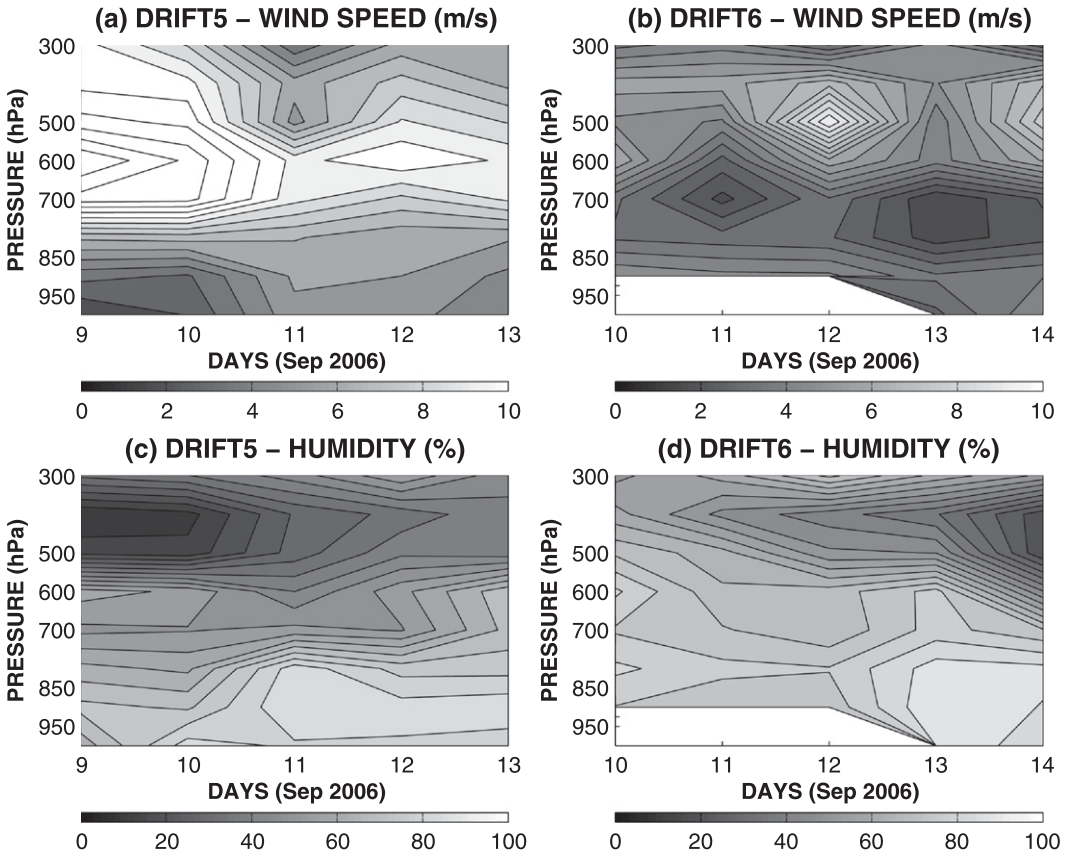

FIG. 14. As in Fig. 4, but for IFS analyses collocated with dropsondes.

are discussed in this article assimilated all additional radiosonde data that were acquired during the AMMA campaign and received via the GTS; excluded are those received from other means of communication (e.g., e-mail). This applies to the experiments that run with the ARPEGE model and to those run with the IFS model. At the time of the assimilation tests, which spreads over the years 2007–09, some other developments were ongoing regarding radiosonde bias corrections. Several coauthors of this article have contributed to some of this work. Therefore all these studies were carried out in parallel and no assimilation experiment, among those conducted during AMMA 2006, combines the developments in the use of data over land (AMSU, MERIS, etc.) and the developments to bias correct the radiosonde data. Corrections to the radiosonde biases were used in the operational ECMWF system since version 32R3 and were estimated using the RS92 radiosonde observations but only from 2007 onward. For the period studied here, radiosonde data were not bias corrected.

In the present study, we raised some issues in the analysis that deserve careful consideration we would like to do in the near future. However, this comparison exercise has enabled us to highlight some preliminary results. We show that the NWP analyses and forecast are generally in better agreement with data from dropsondes when microwave observations are assimilated over land. However, the comparison also shows the need for a better synergy between the developments on assimilation and those of physical parameterizations. This is needed to prevent the forecast models to lose the benefit of better initial state, as shown with the comparison between CY32T0 and CY33T1, which quantifies the contribution of improved physical parameterizations for assimilation.

Conditional sampling over the Saharan air layer (SAL) shows that IFS and ARPEGE represent very well the vertical structure of the SAL and the associated very dry layers, with a slightly better performance for IFS (the departure bias from dropsondes at 850 hPa is close to 1.6% and to −2.6% for IFS and ARPEGE, respectively). This is encouraging for the ability of models to predict these intense events in the tropics that are an essential source of modulation of tropical cyclogenesis. However, SAL events are a surge of dusty and dry air over the Atlantic. The absence of aerosol representation

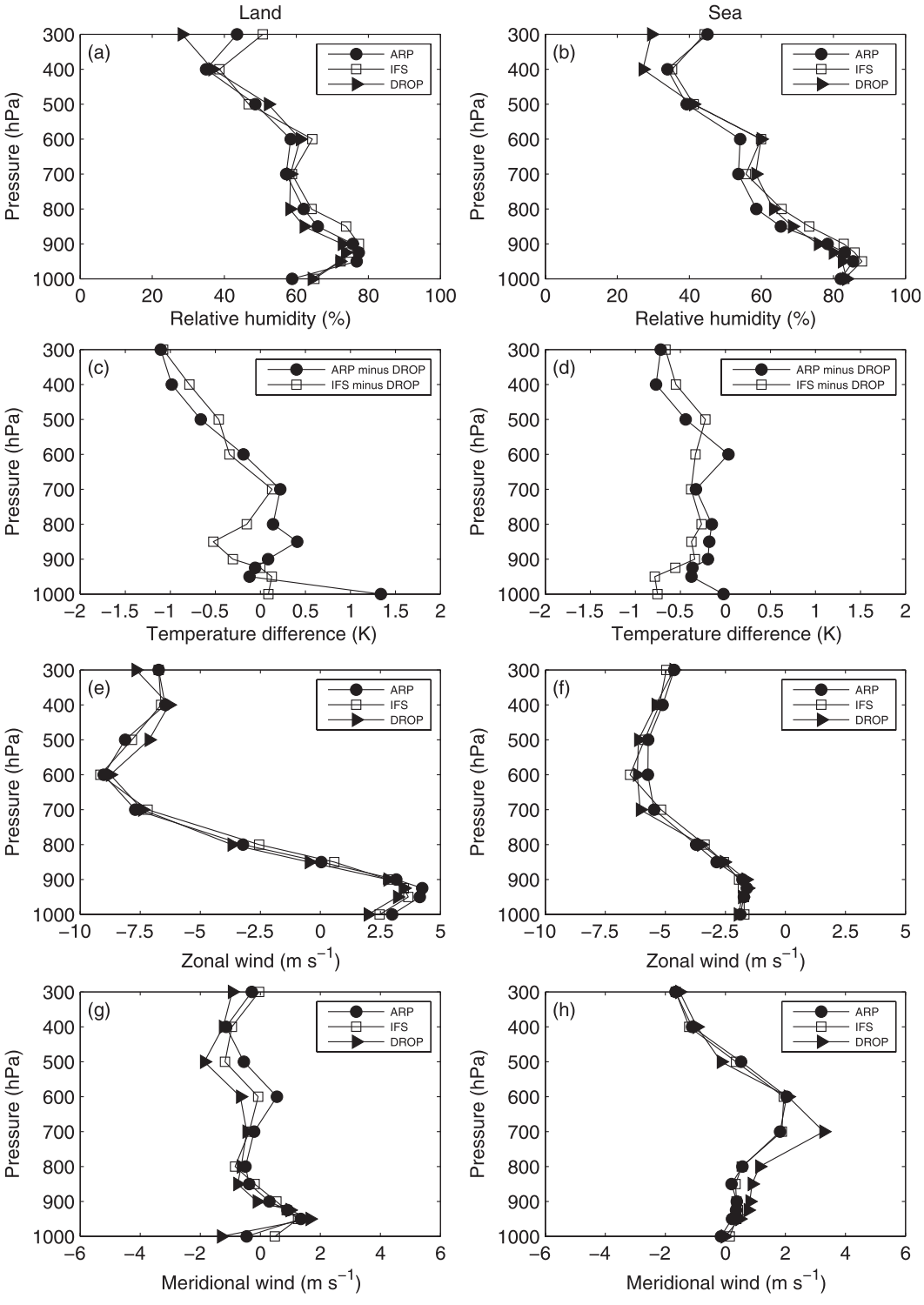

FIG. 15. Vertical profiles of (a),(b) relative humidity, (c),(d) temperature difference, (e),(f) zonal wind, and (g),(h) meridional wind from ARP33-EXP and IFS-EXP analyses collocated with dropsondes over (left) land and (right) the sea.

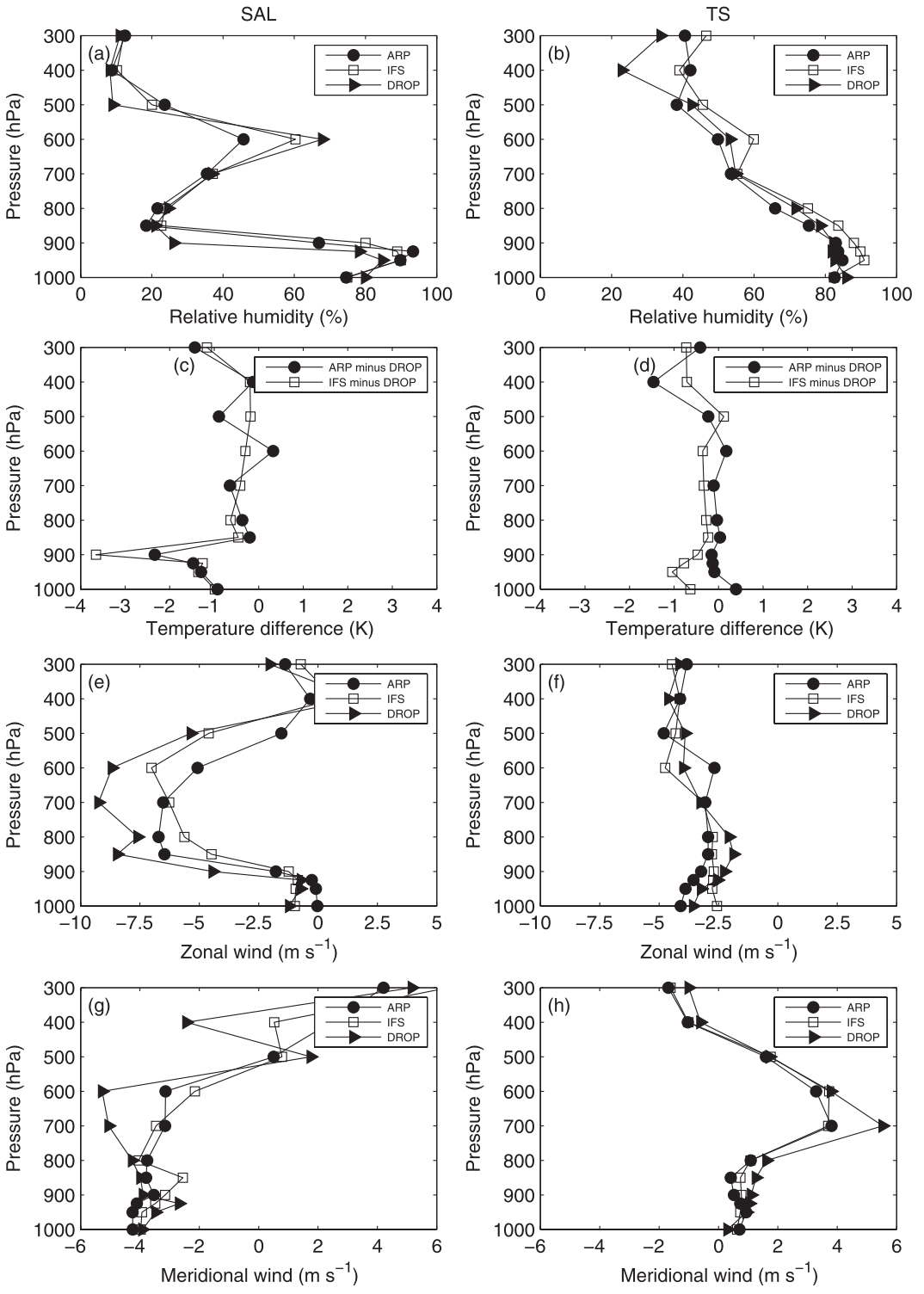

FIG. 16. As in Fig. 15, but for (left) SAL and (right) TS environments.

in the NWP models might be a key for future NWP model development. Indeed, both ARPEGE and IFS display simulated cold temperature bias in the low layers of the SAL that could be partly attributed to the absence of aerosol radiative heating in the NWP models. Conditional sampling of the tropical storm environment shows that both IFS and ARPEGE represent well the vertical structure of moisture, temperature, and also

wind. The two models simulate surprisingly fairly weak near-surface winds with nearly no vertical shear, in agreement with the observations, as well as a nearly saturated and deep planetary boundary layer.

However, the weak ability to predict the meridional wind is a common feature of ARPEGE and IFS. It has been raised without succeeding in identifying the cause of this low score and its implications on the simulation of the regional atmospheric circulation and associated extreme weather like TS. Indeed, the problem does not appear to be corrected by the assimilation of more observations. It must be stressed that the inability of the models to adequately represent the meridional wind could not be detected using a conventional diagnostic evaluation of the analysis and forecast, thus illustrating the importance of independent nonassimilated data from validation. This highlights the need for dedicated field campaigns like AMMA. Finally, there is a need for a more intensive use of remote sensing observations. At present, a large amount of microwave observations are assimilated over land but only in clear-sky situations. More work has to be conducted to also assimilate observations in cloudy conditions. Unlike Météo-France, ECMWF has already assimilated microwave observations in cloudy and rainy conditions, but only over the sea. Moreover, it would be highly useful to review the present intercomparison by looking through the relationship between biases in temperature/humidity and the representation of high/low clouds in both systems.

Finally, the driftsonde system has been specifically designed for data-sparse regions such as oceans and sparsely populated or underdeveloped regions generally lacking such observations (e.g., part of the THORPEX concept). At the time of initial development, the available dataset was more satellite based over the ocean and heavily influenced by in situ data over land. This paper stresses the need of additional in situ observations over oceans to test satellite techniques over land. Since AMMA was the first large field experiment in which driftsonde systems have been deployed, it is worth emphasizing that all the driftsondes deployed were still on probation, and the mission success rate was fairly low (about 50% successful dropsondes). The system has been improved in the THORPEX Pacific Asian Regional Campaign (T-PARC) in 2008 and Concordiasi in 2010 with the addition of pressure sensor and a mission success rate reaching 95% (Drobinski et al. 2013).

Acknowledgments. We are thankful to J. P. Lefebvre (CNES), A. Hertzog and R. Roca (IPSL/LMD), J. Fox, K. Romberg, J. Van Andel, H. Cole, C. Martin, G. Granger, D. Flanigan, and D. Lauritsen (NCAR) for assistance in operation of the driftsonde system. Based on a French initiative, AMMA was built by an international scientific group and is currently funded by a large number of agencies, especially from France, the United Kingdom, Germany, the United States, and Africa. It has been the beneficiary of a major financial contribution from the European Community's Sixth Framework Research Program. Detailed information on scientific coordination and funding is available on the AMMA International website http://www.amma-international.org.

REFERENCES

Agusti-Panareda, A., and Coauthors, 2009: Radiosonde humidity bias correction over the West African region for the special AMMA reanalysis at ECMWF. *Quart. J. Roy. Meteor. Soc.,* **135,** 595–617.

——, A. Beljaars, C. Cardinali, I. Genkova, and C. D. Thorncroft, 2010: Impact of assimilating AMMA soundings on ECMWF analyses and forecasts. *Wea. Forecasting,* **25,** 1142–1160.

Andersson, E., and Coauthors, 2007: Analysis and forecast impact of the main humidity observing systems. *Quart. J. Roy. Meteor. Soc.,* **133,** 1473–1485.

Bauer, P., 2009: 4D-Var assimilation of MERIS total column water-vapour retrievals over land. *Quart. J. Roy. Meteor. Soc.,* **135,** 1852–1862.

Bechtold, P., E. Bazile, F. Guichard, P. Mascart, and E. Richard, 2001: A mass flux convection scheme for regional and global models. *Quart. J. Roy. Meteor. Soc.,* **127,** 869–886.

Berry, G. J., and C. Thorncroft, 2005: Case study of an intense African easterly wave. *Mon. Wea. Rev.,* **133,** 752–766.

Bock, O., M. N. Bouin, A. Walpersdorf, J. P. Lafore, S. Janicot, F. Guichard, and A. Agusti-Panareda, 2007: Comparison of ground-based GPS precipitable water vapour to in independent observations and NWP model reanalyses over Africa. *Quart. J. Roy. Meteor. Soc.,* **133,** 2011–2027.

Braun, S. A., 2010: Reevaluating the role of the Saharan air layer in Atlantic tropical cyclogenesis and evolution. *Mon. Wea. Rev.,* **138,** 2007–2037.

Carlson, T. N., 1969: Some remarks on African disturbances and their progress over the tropical Atlantic. *Mon. Wea. Rev.,* **97,** 716–726.

Chaboureau, J. P., and Coauthors, 2011: Long-range transport of Saharan dust and its radiative impact on precipitation forecast: A case study during the Convective and Orographically-Induced Precipitation Study (COPS). *Quart. J. Roy. Meteor. Soc.,* **137,** 236–251.

Cook, K. H., 1999: Generation of the African easterly jet and its role in determining West African precipitation. *J. Climate,* **12,** 1165–1184.

Courtier, P., J. N. Thépaut, and A. Hollingsworth, 1994: A strategy for operational implementation of 4D-Var using an incremental approach. *Quart. J. Roy. Meteor. Soc.,* **120,** 1321–1387.

Cuxart, J., P. Bougeault, and J. L. Redelsperger, 2000: A turbulence scheme allowing for mesoscale and large-eddy simulations. *Quart. J. Roy. Meteor. Soc.,* **126,** 1–30.

Drobinski, P., B. Sultan, and S. Janicot, 2005: Role of the Hoggar massif on the West African monsoon onset. *Geophys. Res. Lett.,* **32,** L01705, doi:10.1029/2004GL020710.

——, and Coauthors, 2006: Des ballons stratosphériques traquent la mousson Africaine (Stratospheric balloons track the African monsoon). *Meteorologie,* **55,** 2–3.

——, S. Bastin, S. Janicot, O. Bock, A. Dabas, P. Delville, P. Reitebuch, and B. Sultan, 2009: On the late northward propagation of the West African monsoon in summer 2006 in the region of Niger/Mali. *J. Geophys. Res.,* **114,** D09108, doi:10.1029/2008JD011159.

——, P. Cocquerez, A. Doerenbecher, T. Hock, C. Lavaysse, D. Parsons, J. L. Redelsperger, and S. Vénel, 2013: Hurricane and monsoon tracking with driftsondes. *Earth System Monitoring: Selected Entries from the Encyclopedia of Sustainability Science and Technology,* J. Orcutt, Ed., Springer, 181–197.

Dunion, J. P., and C. S. Velden, 2004: The impact of the Saharan air layer on Atlantic tropical cyclone activity. *Bull. Amer. Meteor. Soc.,* **85,** 353–365.

Faccani, C., and Coauthors, 2009: The impacts of AMMA radiosonde data on the French global assimilation and forecast system. *Wea. Forecasting,* **24,** 1268–1286.

Fink, A. H., and A. Reiner, 2003: Spatiotemporal variability of the relation between African easterly waves and West African squall lines in 1998 and 1999. *J. Geophys. Res.,* **108,** 4332, doi:10.1029/2002JD002816.

Hagos, S. M., and K. H. Cook, 2007: Dynamics of the West African monsoon jump. *J. Climate,* **20,** 5264–5284.

Hall, N. M. J., G. N. Kiladis, and C. D. Thorncroft, 2006: Three-dimensional structure and dynamics of African easterly waves. Part II: Dynamical modes. *J. Atmos. Sci.,* **63,** 2231–2245.

Hertzog, A., F. Vial, C. R. Mechoso, C. Basdevant, and P. Cocquerez, 2002: Quasi-Lagrangian measurements in the lower stratosphere reveal an energy peak associated with near-inertial waves. *Geophys. Res. Lett.,* **29,** L1229, doi:10.1029/2001GL014083.

Janicot, S., and Coauthors, 2008: Large-scale overview of the summer monsoon over West Africa during the AMMA field experiment in 2006. *Ann. Geophys.,* **26,** 2569–2595.

Karbou, F., E. Gérard, and F. Rabier, 2006: Microwave land emissivity and skin temperature for AMSU-A and -B assimilation over land. *Quart. J. Roy. Meteor. Soc.,* **132,** 2333–2355.

——, N. Bormann, and J. N. Thépaut, 2007: Towards the assimilation of satellite microwave observations over land: Feasibility studies using SSMI/S, AMSU-A and AMSU-B. NWPSAF Tech. Rep., 37 pp.

——, F. Rabier, J. P. Lafore, J. L. Redelsperger, and O. Bock, 2010: Global 4D-Var assimilation and forecast experiments using AMSU observations over land. Part II: Impact of assimilating surface sensitive channels on the African monsoon during AMMA. *Wea. Forecasting,* **25,** 20–36.

Karyampudi, V. M., and T. N. Carlson, 1988: Analysis and numerical simulations of the Saharan air layer and its effect on easterly wave disturbances. *J. Atmos. Sci.,* **45,** 3102–3136.

——, and H. F. Pierce, 2002: Synoptic-scale influence of the Saharan air layer on tropical cyclogenesis over the eastern Atlantic. *Mon. Wea. Rev.,* **130,** 3100–3128.

Knippertz, P., and A. H. Fink, 2008: Dry-season precipitation in tropical West Africa and its relation to forcing from the extratropics. *Mon. Wea. Rev.,* **136,** 3579–3596.

——, and ——, 2009: Prediction of dry-season precipitation in tropical West Africa and its relation to forcing from the extratropics. *Wea. Forecasting,* **24,** 1064–1084.

Krzeminski, B., N. Bormann, F. Karbou, J.-N. Thepaut, A. McNally, and P. Bauer, 2008: Towards better usage of AMSU observations over land at ECMWF. *Proc. 16th Int. TOVS Study Conf.,* Angra dos Reis, Brazil, WMO, 345. [Available online at http://cimss.ssec.wisc.edu/itwg/itsc/itsc16/report/ITSC_16_Proceedings.pdf.]

Lavaysse, C., A. Diedhiou, H. Laurent, and T. Lebel, 2006: African easterly waves and convective activity in wet and dry sequences of the West African monsoon. *Climate Dyn.,* **27,** 319–332.

——, J. P. Chaboureau, and C. Flamant, 2011: Dust impact on the West African heat low in summertime. *Quart. J. Roy. Meteor. Soc.,* **137,** 1227–1240, doi:10.1002/qj.844.

Lemaître, C., C. Flamant, J. Cuesta, J. C. Raut, P. Chazette, P. Formenti, and J. Pelon, 2010: Radiative heating rates profiles associated with a springtime case of Bodélé and Sudan dust transport over West Africa. *Atmos. Chem. Phys.,* **10,** 8131–8150.

Leroux, S., N. M. J. Hall, and G. N. Kiladis, 2010: A climatological study of transient-mean-flow interactions over West Africa. *Quart. J. Roy. Meteor. Soc.,* **136,** 397–410.

Mekonnen, A., C. D. Thorncroft, and A. R. Aiyyer, 2006: Analysis of convection and its association with African easterly waves. *J. Climate,* **19,** 5405–5421.

Meynadier, R., O. Bock, F. Guichard, A. Boone, P. Roucou, and J. L. Redelsperger, 2010a: West African monsoon water cycle: 1. A hybrid water budget data set. *J. Geophys. Res.,* **115,** D19106, doi:10.1029/2010JD013917.

——, ——, S. Gervois, F. Guichard, J. L. Redelsperger, A. Agusti-Panareda, and A. Beljaars, 2010b: West African monsoon water cycle: 2. Assessment of numerical weather prediction water budgets. *J. Geophys. Res.,* **115,** D19107, doi:10.1029/2010JD013919.

Nicholson, S., and J. Grist, 2003: The seasonal evolution of the atmospheric circulation over West Africa and equatorial Africa. *J. Climate,* **16,** 1013–1030.

Nuret, M., J. Lafore, O. Bock, F. Guichard, J. L. Redelsperger, A. Agusti-Panareda, and J. B. Ngamini, 2008: Correction of humidity bias for Vaisala RS80 sondes during AMMA 2006 observing period. *J. Atmos. Oceanic Technol.,* **25,** 2152–2158.

Payne, S. W., and M. M. McGarry, 1977: The relationship of satellite inferred convective activity to easterly waves over West Africa and the adjacent ocean during Phase III of GATE. *Mon. Wea. Rev.,* **105,** 413–420.

Rabier, F., H. Järvinen, E. Klinker, J. F. Mahfouf, and A. Simmons, 2000: The ECMWF operational implementation of four-dimensional variational assimilation. I: Experimental results with simplified physics. *Quart. J. Roy. Meteor. Soc.,* **126,** 1143–1170.

Ramel, R., H. Gallée, and C. Messager, 2006: On the northward shift of the West African monsoon. *Climate Dyn.,* **26,** 429–440.

Redelsperger, J. L., C. D. Thorncroft, A. Diedhiou, T. Lebel, D. J. Parker, and J. Polcher, 2006: African Monsoon Multidisciplinary Analysis: An international research project and field campaign. *Bull. Amer. Meteor. Soc.,* **87,** 1739–1746.

Roca, R., J. P. Lafore, C. Piriou, and J. L. Redlesperger, 2005: Extratropical dry-air intrusions into the West African monsoon midtroposphere: An important factor for the convective activity over the Sahel. *J. Atmos. Sci.,* **62,** 390–407.

Shapiro, M. A., and A. J. Thorpe, 2004: THORPEX international science plan. WMO/TD 1246, WWRP/THORPEX 2, 51 pp.

Sijikumar, S., P. Roucou, and B. Fontaine, 2006: Monsoon onset over Sudan-Sahel: Simulation by the regional scale model MM5. *Geophys. Res. Lett.,* **33,** L03814, doi:10.1029/2005GL024819.

Solmon, F., M. Mallet, N. Elguindi, F. Giorgi, A. Zakey, and A. Konaré, 2008: Dust aerosol impact on regional precipitation over western Africa, mechanism and sensitivity to absorption properties. *Geophys. Res. Lett.,* **35,** L24705, doi:10.1029/2008GL035900.

Sultan, B., and S. Janicot, 2003: The West African monsoon dynamics. Part II: The preonset and onset of the summer monsoon. *J. Climate,* **16,** 3407–3427.

——, ——, and P. Drobinski, 2007: Characterization of the diurnal cycle of the West African monsoon around the monsoon onset. *J. Climate,* **20,** 4014–4032.

Thorncroft, C. D., N. M. J. Hall, and G. N. Kiladis, 2008: Three-dimensional structure and dynamics of African easterly waves. Part III: Genesis. *J. Atmos. Sci.,* **65,** 3596–3607.

Tompkins, A. M., and L. Feudale, 2010: Seasonal ensemble predictions of West African monsoon precipitation in the ECMWF system 3 with a focus on the AMMA special observing period in 2006. *Wea. Forecasting,* **25,** 768–788.

——, C. Cardinali, J. J. Morcrette, and M. Rodwell, 2005: Influence of aerosol climatology on forecasts of the African easterly jet. *Geophys. Res. Lett.,* **32,** L10801, doi:10.1029/2004GL022189.

Veersé, F., and J. N. Thépaut, 1998: Multiple truncation incremental approach for four-dimensional variational data assimilation. *Quart. J. Roy. Meteor. Soc.,* **124,** 1889–1908.

Zipser, E. J., and Coauthors, 2009: The Saharan air layer and the fate of African easterly waves: The NASA's AMMA field study of tropical cyclogenesis. *Bull. Amer. Meteor. Soc.,* **90,** 1137–1156.